EXHIBIT E

A. SPECIFIC AIMS:

Altered brain iron metabolism in the face of aging is cited as a significant risk factor for "oxidative stress," neuronal death, and the development of Alzheimer's disease (AD). Preliminary work presented in this proposal will document our novel approach to detecting abnormalities in cellular iron homeostasis by both *ex vivo* peripheral blood testing and unique brain magnetic resonance imaging (MRI) technology.

Hypothesis: Following the dementing clinical course of a cohort of mildly cognitively impaired (MCI) subjects will reflect iron regulatory and "oxidative stress" anomalies detectable in their circulating peripheral blood leukocytes and in the brain by special phase MR imaging.

In a collaborative, interdisciplinary initiative, this proposal seeks to expand our preliminary studies by exploring the following specific aims.

1) Define *ex vivo* markers for AD in peripheral blood leukocytes of MCI and control subjects by flow cytometric, immunocytochemical identification of the iron sensing peptide domain of iron regulatory protein-2 (IRP-2), amyloid precursor protein (APP), spontaneous and stimulated apoptosis, and cytokine expression by multiplexed flow cytometric analysis. Identify IRP-2 polymorphisms in the iron-sensing loop of the IRP-2 gene using RT-PCR and posttranslational modification of IRP-2 protein using monoclonal antibodies.

2) Develop new magnetic resonance imaging (MRI) technology for quantification and monitoring of brain iron in its various *in vivo* states (non-transferrin bound iron-NTBI, transferrin bound iron-TBI, and high molecular weight complexes – ferritin, hemosiderin). An experimental mouse model has been genetically engineered with a targeted deletion of IRP-2, causing these mice to accumulate brain iron and develop a neurodegenerative disorder. This model will serve to validate our *ex vivo* blood markers and our new MR imaging technology by quantitative histochemical assays of iron in its various steady state correlations.

3) Combine the data obtained in Aims 1 and 2 with periodic psychometric evaluations of the subject population (MCI) at risk for AD to determine relationships and/or correlations between the serial *ex vivo* blood markers, MR iron quantitation, and clinical course.

B. BACKGROUND AND SIGNIFICANCE:

B.1. A summary of existing information that pertains to brain iron and AD will be presented in this section as it relates to our specific aims. There are four important unanswered questions regarding brain iron and neurodegenerative disease that this proposal may help to resolve:

1) **Is iron accumulation in the MCI brain a primary or secondary event leading to AD?**
2) **Are polymorphisms in Iron Regulatory Proteins (IRP's) responsible for iron accumulation in AD?**
3) **Can special MRI of the brain quantitate and monitor iron in its various states – an application not only for AD but other neurodegenerative disorders?**
4) **Do alterations in leukocyte biology reflect iron-related biochemical changes in the brain in AD and can these markers be used as prognosticators in MCI?**

Our study of MCI and AD utilizes a unique approach that is necessary to begin answering these important questions. We believe the answers lie in defining the molecular mechanisms of iron-mediated "oxidative stress" in cellular systems that replicate *in vivo* steady state brain circumstances.

Furthermore, there is a need to define brain iron accumulation in quantitative terms. **Patients with MCI deserve selective attention so that initiating factors may be identified and therapy instituted prior to the devastating consequences of disease.**

The multidisciplinary group that we have assembled has experience in the following areas: diagnosis and therapy of dementing illnesses, immunocytochemistry, flow cytometry, cytokine biology, leukocyte biology, development of diagnostic immunoassays and biological assays, molecular events governing iron homeostasis, physics and diagnostic interpretation of MRI, molecular genetics, and biostatistics. The anticipated solutions to the above-cited questions are expanded on below.

B.2.1. *Ex vivo* markers for AD

Alzheimer's Disease is the end result of an array of biochemical changes in the neurons of affected patients each contributing to the eventual development of pathology. These alterations may include: over-expression of βAPP providing the raw material for Aβ, heightened expression or activity of presenilins which cleave the βAPP into Aβ, reduced activity of Aβ digesting enzymes like neprilysin, clogging and overloading of the ubiquitin/proteosome system, inhibition of repair mechanisms associated with APOE4 isoforms, creation of tau protein tangles which may alter the cytoskeleton and function of neurons, and altered activity of iron regulatory proteins which overload the cells with iron and contribute to oxidative damage and the creation of reactive oxidative species (ROS). These changes lead to the development of inflammation and oxidative stress damage. The ability to develop useful *ex vivo* markers may require the quantitation and correlation of a number of these contributory factors.

The criteria for an ideal biomarker for AD has been defined in a consensus report entitled: "Molecular and Biochemical Markers of Alzheimer's Disease" (1). The biomarker should detect a fundamental feature of the neuropathology, have a sensitivity of >80% for detecting AD, and a specificity of >80% for differentiating other dementias. Rare cases of early-onset familial AD warrant testing for genetic aberrations (presenilin1, presenilin2, and APOE), but these indicators are not useful in late onset and sporadic AD. **Validation with control groups for age and gender distribution identical to the subject group is difficult to fulfill with elderly patients. Sporadic AD affects the elderly, so purported controls or MCI subjects may have preclinical AD.** Thus no *ex vivo* biomarker in the elderly for sporadic AD can be 100% sensitive and specific. A report of elevated iron binding protein p97 in the peripheral blood of AD patients has not been confirmed (2). Other serum and body fluid neurochemical markers touted as diagnostic for AD include nerve growth factor (3), and cerebrospinal fluid $A\beta_{42}$ and tau protein (4). The latter two CSF markers are considered closest to fulfilling criteria for usefulness (4, 5). A major drawback for the test is the necessity to perform a lumbar puncture on the target population.

B.2.2. In short, there are no currently accepted biomarkers for AD or MCI.

In spite of this, we feel there is sufficient evidence that a diagnostic paradigm can be developed for AD and other neurodegenerative diseases by quantitating and correlating combined analysis of a number of different protein markers and changes in biological activity of peripheral blood leukocytes.

In determining whether *ex vivo* markers for AD can be found in the peripheral blood, it should be noted that there is convincing evidence pointing to the fact that the biological activity of peripheral blood lymphocytes, platelets and macrophages can be affected in patients with AD (6). Additionally, proteins associated with AD have been identified in peripheral blood leukocytes and appear to have a role in normal physiology. This suggests the potential of these cells as sources of *ex vivo* markers that could be used as identifiers for AD. Recent studies have identified isoforms of

βAPP present as integral membrane proteins in peripheral blood leukocytes and platelets and their up-regulated expression in AD (6). Additionally, cleavage of the βAPP into Aβ and its cytoplasmic peptide tail results in activation of gene transcription in response to the peptide, suggesting a normal physiological function and a role in the modification of leukocyte biological activity (7). IRP-2, a critical protein regulating uptake and processing of iron in neurons has also been identified in leukocytes (our observation) and may play a significant role in the creation of ROS from Aβ peptides. There are several characteristics of leukocytes from aging individuals that peripherally may reflect biochemical changes in the brain that are associated with AD. These changes include chronic expression of activation markers such as HLA-DR and CD95 (the receptor for FAS ligand and an inducer of apoptosis)(8), increased spontaneous apoptosis, increased susceptibility to oxidative stress damage and subsequent apoptosis (9), and diminished immune response concurrent with reduction in the production of growth inducing cytokines like Interleukin-2 (10). Several of these changes are present in patients with AD while not present in cases of vascular dementia.

B.2.3. Iron mediated "oxidative stress" and AD

The accumulation of iron in the brain is increasingly implicated as a risk factor for AD, but remains an unproven hypothesis (2, 11-14). Circumstantial evidence supporting this speculation is based on the study of necropsy material – showing iron in elevated amounts in the pathologic hallmarks of AD [senile plaques (SP) and neurofibrillary tangles (NFT's)]. Iron accumulation occurs regionally in brain areas associated with memory (hippocampus, amygdala, nucleus basalis Meynert's, and cerebral cortex). Important questions remain unanswered e.g. why are iron levels high in these regions? Is iron accumulation a primary or a secondary "oxidative stress," event? What are the steady state levels of the variable iron states *in vivo*? Answers to these fundamental questions require new analytical paradigms and cannot be achieved by the study of necropsy material or *in vitro* assays that bear only indirect relationship to endogenous events.

The basis for the iron mediated "oxidative stress" hypothesis is the presence in the AD brain of oxidized proteins, carbohydrates, lipids and nucleic acids and *in vitro* production of NFT's by oxidative modification of proteins (15-19). Though responsible molecular oxidation mechanisms remain unverified, free ferrous iron (Fe^{++}) has been demonstrated to convert Aβ peptide to an oxidizing free radical. "Radicalized" Aβ can illicit an inflammatory and complement-mediated cytolytic response. Microglial activation can result in the expression of pro-inflammatory cytokines and lead to further "oxidative stress"(20, 21).

Iron is a necessary element in many normal cellular functions in peripheral blood leukocytes. This is especially evident during cell activation where there is a significant and prolonged increase in transferrin receptor expression. Normal circulating leukocytes express insignificant levels of transferrin receptors. Upon activation with antigens or mitogens, expression of transferrin receptors is increased more than one hundred fold (22). This facilitates uptake of iron necessary for cell division and other cellular functions. Missregulation of iron associated with IRP-2 could be secondary to intrinsic overexpression of intracellular IRP-2, due to reduced ubiquitination of IRP-2 and proteosomic removal, or direct inhibition of the proteosome. **Each of these potential errors could result in prolonged expression of IRP-2 and maintenance of cellular metabolism in the iron-loading mode.**

Preliminary studies using phycoerythrin-labeled monoclonal antibodies directed against a peptide representing the loop region of the wild-type IRP-2 protein has demonstrated some differences in the intrinsic expression of IRP-2 in some patients with AD. **Comparatively, continuously growing cell lines, such as the KG-1 human myeloid leukemia cell line, constitutively over-express transferrin receptors and have been demonstrated in our laboratory to have heightened expression of IRP-2 in comparison to resting lymphocytes** (Preliminary Data Section C, Figures 3, 4, and 5). Differences

in intrinsic expression of IRP-2 in resting lymphocytes from AD patients could be indicative of either intrinsic over-expression of IRP-2 or reduction in proteosomic removal. β-Amyloid proteins have been identified as inhibitors of the proteosome, overexpression of these peptides and their precursor form as an integral membrane protein could provide the raw materials for proteosome inhibition (6). Identification of overexpression or of mutations in the IRP-2 protein in AD used in conjunction with the expression of cell surface βAPP could have potential for *ex vivo* biomarkers for AD.

Iron, particularly in its bivalent state, is known to participate in the generation of potent reactive oxidant species (ROS), particularly the hydroxyl free radical (17, 23). Ferrous iron is toxic whereas iron in the ferric state is relatively insoluble and non-reactive. Non-heme iron exists in the brain in three different forms: "low molecular weight" complexes or non-transferrin bound iron (NTBI), iron bound to medium molecular weight complexes to form metalloproteins (transferrin), TBI, and the high molecular weight complexes of ferritin and hemosiderin (24, 25). Iron in the "free" or NTBI state, in the bivalent or trivalent state is highly reactive and participates in the generation of hydroxyl free radicals. Ferritin, the iron storage protein, can rapidly release or take up iron and thus can be interpreted as either a potentially harmful iron donor (23, 26, 27) or as an anti-oxidant defense (13, 27). Studies of "oxidative stress" in other systems (liver) point out the dynamic and rapidly responsive and changing levels of tissue iron between the three states "free" or NTBI, TBI, and ferritin (28). Attempts to extrapolate back to *in vivo* circumstances in the AD brain from analysis of dead brain is artifactual and accounts for the lack of a convincing molecular explanation. The ability to measure iron levels in its various forms in the absence of post-necrotic changes could aid in the determination of the role of iron in AD.

B.2.4. The Post-Transcriptional Control of Brain Iron Homeostasis: The Iron Regulatory Proteins

Cytosolic levels of brain iron in its three non-heme states are tightly controlled since the element is bifunctional; an essential nutrient or a potential toxin (13, 23, 27). **IRP-1 and IRP-2 are distinct, but homologous proteins that serve as iron sensors to coordinate cellular iron uptake, storage, and incorporation into proteins.** This coordination is an example of a post-transcriptional control mechanism. IRP's bind to RNA transcripts for transferrin, transferrin receptor, and ferritin that have stem loop structures referred to as an iron responsive elements (IRE's). Binding controls both the rate of mRNA translation and stability. A balance between the mRNA directed protein synthesis of either ferritin (for iron storage in iron replete cells) or transferrin and receptor (TfR) maintains iron homeostasis in the cell. IRE's are located in the 5'-untranslated region (5'-UTR) of mRNA encoding ferritin and the 3'-untranslated (3'-UTR) of the mRNA encoding TfR. IRP binding to the 5'-UTR represses translation of ferritin biosynthesis. On the other hand IRPs binding to the 3'-UTR stabilizes the mRNA and enhances TfR synthesis. Intracellular iron levels regulate the concentration of IRP's by altering activity of IRP-1 and stability of IRP-2. IRP-2 is rapidly degraded in iron replete cells, and thus is only available for transcript binding in iron-depleted cells. The result is repression of ferritin synthesis and enhanced TfR synthesis mediating iron uptake when iron levels are low. In the presence of excess cellular iron, RNA binding of IRP's is decreased resulting in an increase in ferritin and increased rate of degradation of TfR mRNA (29)(30).

In AD brains IRP-2 has been determined by immunohistochemistry to co-localize with intraneuronal lesions, NFT's, SP's, neuropil threads, and redox-acting iron (NTBI). These immunocytochemical observations, measured AD IRP binding activity to mRNA iron regulating elements, and increased brain iron without a concomitant increase in ferritin is speculated to be the result of an "abnormal" or "altered IRP-2"(31, 32). **Our hypothesis is that the normal, iron-mediated oxidation mechanism for IRP-2 degradation – a rapid process associated with iron binding to specific cysteine clustered residues**

in the iron sensing domain – is perturbed in AD. In other words, increased levels of IRP-2 in the face of increased cytosolic iron results in continuous cellular iron uptake and eventual toxicity.

There is sufficient evidence to suggest that IRP-2 plays a role in iron metabolism in leukocytes. Immune activation of leukocytes is associated with up-regulation of transferrin receptors and uptake of iron (33). It is assumed that if altered transcripts of IRP-2 are present in the neurons that those alterations would be reflected in the peripheral blood leukocytes. If ubiquitination of mutant IRP-2 is inhibited, it is anticipated that enhanced levels of mutant IRP-2 protein should be retained after activation in contrast to native IRP-2 and could be detected in activated leukocytes from patients with AD. Additionally, it would be anticipated that there would be increased basal levels of cell surface transferrin receptors on peripheral blood leukocytes associated with chronic low level activation and the stabilization of transferrin receptor expression secondary to the activity of IRP-2. This has not been previously investigated. Prolonged expression of IRP-2 in AD would be associated with stabilization of transferrin receptor expression and subsequent uptake of iron by cells. Without a concomitant increase in ferritin production free iron could build to toxic levels in the cells resulting in neuronal cell death. The potential increase in basal levels of transferrin receptors on peripheral blood leukocytes could easily be studied by flow cytometry using fluorochrome-labeled transferrin to identify cells possessing functional transferrin receptors. This system has already been well developed by the laboratories at BioErgonomics Inc. and would be investigated in conjunction with expression of IRP-2.

The availability of cell surface βAPP, the presence of enzymes to cleave the precursor into $A\beta_{40}$ and $A\beta_{42}$, in conjunction with intracellular IRP-2 overexpression or mutations in peripheral blood leukocytes of AD patients could result in the production of toxic ROS and could potentially be associated with observed increases in spontaneous and activation-induced apoptosis (34). The missregulation of iron by mutant or overexpressed IRP-2 in peripheral blood leukocytes and subsequent oxidative damage could initiate post-activation apoptosis or necrosis and could potentially serve as an *in vitro* model for neuronal cell death in AD (35).

Cellular IRP-2 levels are regulated by iron binding to a defined peptide loop formed by amino acids 136-216 harboring 3 cysteine residues in close physical grouping (30)(36). Iron binding to this sulfhydryl cluster results in a controlled oxidation that results in rapid degradation of the molecule by generating signals for ubiquitination and proteosomal processing. The molecular mechanisms governing this controlled protein oxidation are currently being investigated in our laboratory in collaboration with the laboratories of Dr. Rodney Levine and Dr. Tracey Rouault and will be discussed in preliminary studies. Our goal is to evaluate peripheral circulating leukocytes that undergo "oxidative stress" and apoptosis in order to search for aberrations in IRP-2 structure. Development of monoclonal antibodies specific for the potential mutated cysteine residues present in the loop region could provide the necessary tools to investigate the role of these mutations in altered iron metabolism in AD. Identification of the specific mutations associated with AD could provide the means to produce mice expressing these specific mutations and investigating the *in vivo* biological consequences of these mutations.

Inflammation has been assumed to play an important role in the pathology of AD (37, 38). Inflammatory responsiveness is regulated by the production of pro- and anti-inflammatory cytokines. It is worth investigating whether chronic production of pro-inflammatory cytokines plays a role in AD and in addition whether that could be used as an *ex vivo* marker of AD. The most prominent cytokines associated with inflammatory responses are Interleukin-1 (IL-1), Interleukin-6 (IL-6), Tumor Necrosis Factor (TNF) and the chemokines (39, 40). Interestingly, TNF is also associated with induction of apoptosis via binding to the TNF cell surface receptor and activation of apoptosis via activation of the death domain (TRADD) and the death factor (TRAF-2) and could play some role in AD-associated neuronal cell death. Identification of cell surface βAPP on peripheral blood leukocytes, increased susceptibility to oxidative stress and spontaneous apoptosis, and the identification of leukocyte-derived

isoforms of βAP in amyloid plaques strongly suggest a role of inflammatory cells in the pathogenesis of AD. **Using assay systems developed in the laboratories of BioErgonomics Inc., the production of these three prominent pro-inflammatory cytokines by peripheral blood leukocytes will be studied in AD patients and compared to young subjects and age-matched normals by a highly specific and sensitive flow cytometric analysis.** This will be accomplished by isolation of blood mononuclear cells from peripheral blood and culturing them under non-stimulatory and stimulatory conditions and measuring the expression of intracellular cytokines in cell subsets and the quantitation of secretion of these cytokines into culture supernatants by a flow cytometric particle-based immunofluorescent assay system capable of quantitating cytokines at the sub-picogram/ml level. Subtle differences in cytokine production by these cells can be detected by this methodology. Standard enzyme-linked immunoassay methods are not capable of accurately quantitating cytokines at levels lower than 20-30 picograms/ml. Absent immune stimulation or inflammation, normal peripheral blood leukocytes do not secrete measurable levels of these cytokines (40). The presence of cytokine production by peripheral blood mononuclear cells in conjunction with elevated cytoplasmic IRP-2, cell surface βAPP, and increased spontaneous apoptosis could potentially provide powerful ex vivo markers for the identification of AD.

The main thrust of the development of *ex vivo* biomarkers for AD will involve coordinating and multiplexing data from expression of cell surface βAPP, intracellular IRP-2 levels, presence of mutations in IRP-2, rate of spontaneous and activation-induced apoptosis, and expression of proinflammatory cytokines in peripheral blood leukocytes from the patient and age-matched control groups. The IRP-2 knockout mouse will provide an additional model for perturbations in IRP-2 dependent iron metabolism as it relates to cytokine biology.

<u>Developing a New MRI Technology to Quantitate and Monitor Brain Iron</u>

B.3.1. Though there are a number of reports of quantitation of brain iron by MRI (41-46), there are no universally accepted methods, standards, and no calibrated or verified data on humans.

What is agreed upon is that serial, longitudinal studies looking for differences in rates of change for example, of temporal lobe and hippocampal volume, are more powerful diagnostic aides than isolated measurements. This has been proven by identifying MRI patterns of temporal lobe atrophy in a longitudinal study of AD patients (47).

Abnormal iron accumulation in the brain occurs in a variety of neurodegenerative disorders - Huntington's disease, Parkinson's disease, Alzheimer's disease, MS near plaques, chronic hemorrhagic cerebral infarction, thalassemia and hemochromatosis. The ability to assess quantitatively regional brain iron sequentially has potential utility in both diagnosis and monitoring of prospective treatments.

Iron has numerous effects on MR images in its paramagnetic form. It leads to signal changes in magnitude and phase images in T2* weighted gradient echo images, to signal changes in T2 weighted and diffusion weighted spin echo images, and to signal increases in T1 weighted images. In gray matter where iron content is high (such as in the central sulcus), it behaves as a T1 reducing contrast agent. **Nevertheless, no one has successfully quantified "MR visible" iron and conventional imaging shows only a small difference between iron in gray matter and white matter.**

One major source of brain iron is ferritin in ferric form. The protein, ferritin, plays a major role in storage and utilization of iron in the brain. Each ferritin molecule consists of different ratios of H (heavy) and L (light) chain subunits. The subunits are coded on different chromosomes, and appear to play different roles in the function of the ferritin molecule. The H-rich ferritin is efficient at iron sequestration and is predominant in organs with high iron utilization and little iron storage. In contrast, L-rich ferritin is efficient at iron nucleation and is associated with iron storage. In the brain, various cell

types contain ferritin isoforms that are consistent with their functional roles. Ferritin has unique magnetic properties and is believed to be the major source of iron-induced changes in MR tissue relaxation times. There is 10 times the amount of ferritin compared to transferrin in the brain and each ferritin molecule can sequester up to 4500 iron atoms. Ferritin is stored in oligodendrocytes, astrocytes, myelin, and microglia. Macrophages can convert ferritin to hemosiderin, another potent paramagnetic substance that generates signal changes in T2* weighted MRI images. Despite this general knowledge, the MRI properties of ferritin are not well understood. The expected field dependence of R2 is the square of the static field. To the contrary, all evidence points to a linear change in R2 with field strength. No model currently describes observed behavior (except for R2* where our static field dephasing model applies). Further, relaxation rates are generally found to be too high to be explained by simple paramagnetism. A recent paper quotes relaxivities of ferritin for R1 of 2.19 +/- 0.05 /s/mg Fe/g, a value consistent with other measurements (46).

The second major source of brain iron is "free" or non-transferrin bound iron (NTBI). Other sources of trapped iron exist but their concentrations are small. The basal ganglia contain more stainable iron than the cerebral hemispheres and white matter. This observation is in agreement with the phase measurements, R2 or R2' data and other measures of brain iron. Brain iron has been assayed post-mortem. Direct assays give iron levels of 5.3 μmol/g dry weight for cerebral cortex to its highest levels in the globus pallidus of 13.5 μmol/g dry weight (48). There is an increase in iron stores in the hippocampus in Alzheimer's disease and Parkinson's disease. Conner et al. made the following observations regarding AD brain: ferritin is present in glia and astrocytes in gray matter but not in white matter; free iron is lower in white matter; gray matter ferritin increases with age while astrocyte iron remains the same (25).

High field results on animals (49) and humans (41-45) have attempted to quantify brain iron. Although they clearly show the trend in R2 to increase as iron content increases, **predictive power is poor**. For example, Fenzi shows that the slope for R2 is 10 to 30 /s/(mg/gm Fe) on a phantom with an R2 of 40/s when there is no iron (49). However, *in vivo*, a single T2 of 150/s can correspond to a range of 1.5 to 3.5 mg Fe/gm wet weight, far too broad to be of clinical value. Similarly, Bonkovsky's data show that a single signal intensity measurement corresponds to a range of 2/mg/gm dry liver for low concentrations and 5/mg/gm dry liver for concentrations above 1/mg/g dry liver (50).

Ordidge and his group demonstrated that the key information lay in R2' not R2 (51). The problem with R2 is that there are other effects that can change T2 that confounds information about local iron. There is an anomalous recovery of signal for long echoes despite the local increase in iron in the substantia nigra, and in these cases R2' continues to increase with an increase in iron content. A method was developed by that group to measure R2' despite the presence of background field variations that dephase the signal and otherwise yield a falsely high value for R2'. This was accomplished by compensating the local field in the slice select direction by repeating the scan multiple times using different slice select gradients. **This method is a significant improvement over past measurements but leads to a much longer scan time and does not account for field inhomogenities in the plane of the scan.**

Gelman et al. (46) measured both R2 and R2' effects and found that the slope of R2 is 60/s/mg wet wt with an intercept 12.7 or T2 of about 80ms, the slope of R2' is 50/s/mg wet wt with an intercept 2.7 (one might postulate that this non-zero intercept may represent the heme iron contribution) and as an example, the R2' of globus pallidus is 12/sec. In fact, a number of papers have demonstrated the T2 and T2* effects of iron in the basal ganglia and liver. Even basic diffusion mechanisms have been used to describe the signal loss with iron. **None has had a successful predictive outcome**. More recently, two groups have developed a theory of spin dephasing in the static or slow diffusion regime (52) and in the fast diffusion regime (53). **Our theory directly suggests a means by which the source of the susceptibility can be quantified through its magnetic moment and volume content.** This unique

feature has been considered when evaluating parallel fibers (54) and to measure oxygen content in the brain (55). The method will be discussed further in the preliminary results and experimental design sections.

B.4.1. Application of These Tests, in Addition to Recommended Psychometric Evaluations, in Serial Fashion to a Subject Population (MCI) at Risk for AD in Order to Establish Correlations Between Serial *ex vivo* Blood Markers, MR Iron Quantitation, and Clinical Course

The mild cognitive disorder or mild cognitive impairment syndrome (MCI) has been identified as a disorder of subthreshold dementia that warrants intensive investigation (56-58). Subjects with this diagnosis perform 1.0 to 1.5 standard deviations below the reference standard for normal individuals on standard neuropsychologic examinations, but are not demented by standard tests. The important issue to resolve is which cases of MCI will remain static and which will rapidly progress into dementia. An important diagnostic issue is that the diversity of dementing syndromes and surgically treatable disorders must be differentiated. "Normal Pressure Hydrocephalus," for example, can be relieved by shunting procedures for CSF (59). Frontal-temporal atrophy and multi-infarct dementia are disorders that can be differentiated from AD.

Subjects at risk for AD display mild cognitive impairment for months to years prior to the aggressive expression of the disorder. The earliest manifestations of AD are deficits in the areas of executive function and memory. Longitudinal follow-up of AD cases with specific discriminating neuropsychological studies increases the diagnostic accuracy for AD, and detailed cognitive testing is probably the most sensitive diagnostic indicator. Cognitive functions that have proven in previous studies to be sensitive indicators for AD have been composite scores covering the domains of memory, executive function, attention, orientation, visual perception and construction (60, 61). These tests form the basis of diagnosing and following AD patients. Neuropsychiatric tests for AD are now well standardized and applicable to both Hispanic and Oriental target populations.

Guidelines and practice recommendations for the early detection of MCI in the elderly have recently been established (56). There is sufficient evidence to conduct clinical monitoring of these patients with screening instruments that include: Mini-Mental State examination, neuropsychologic tests, with supporting data from focused cognitive instruments and close observer information. The importance of future research directed towards identification of the MCI patient has been emphasized, since 6 to 25% of the cases convert to AD yearly (56).

It is anticipated that carefully selected MCI patients will provide a key factor in the development of *ex vivo* markers for AD. Because a high percentage of these patients will progress to AD, the processes that lead to progression will be highly active and most detectable. Differences in *ex vivo* markers between normal age matched controls and MCI patients would probably be most evident at this time.

B.5. Significance of this Proposal: Summary

This study seeks to define the risk factors associated with "oxidative stress" and AD development in a volunteer cohort of 75 subjects with "mild cognitive impairment." This study is unique in that subjects will be followed longitudinally for 3 to 4 years with a panel of new *ex vivo* peripheral blood and MR brain imaging techniques. A genetically engineered mouse that accumulates brain iron and express a neurodegenerative disorder will be used to validate and quantitate steady state levels of brain iron. To achieve our goals we have assembled an interdisciplinary group of investigators that is the particular strength of this proposal. Two recognized authorities on "oxidative stress" (**Dr. Rodney Levine**) and iron metabolism (**Dr. Tracey Rouault**) are participating in this work.

C. PRELIMINARY STUDIES OF OUR PARTNERSHIP:

The proposed research involves a multidisciplinary approach toward defining non-invasive (*ex vivo*) diagnostic testing for early detection of AD and potentially other neurodegenerative diseases. We have established several lines of evidence that place us in a unique position to make serious inroads into solving this problem. The preliminary data section that follows presents the findings that form the basis of our research project.

Specific Aim #1. Define *ex vivo* markers for AD in peripheral blood leukocytes of MCI and control subjects by flow cytometric, immunocytochemical identification of the iron sensing peptide domain of iron regulatory protein-2 (IRP-2), amyloid precursor protein (APP), spontaneous and stimulated apoptosis, and cytokine expression by multiplexed flow cytometric analysis. Identify IRP-2 polymorphisms in the iron-sensing loop of the IRP-2 gene using RT-PCR and posttranslational modification of IRP-2 protein using monoclonal antibodies.

The rationale for this BRP originated when Dr. Rodney Levine (NIH) contacted Dr. Wolff Kirsch in the fall of 1999. Dr. Levine requested access to a monoclonal antibody (mAb) that Dr. Kirsch's laboratory had prepared to aminomalonic acid (β-carboxyglycine) in peptide linkage. Aminomalonic acid (Ama) and β-carboxyaspartic acid were identified in nature for the first time by Dr. Kirsch and his colleagues (62). See Figure 1.

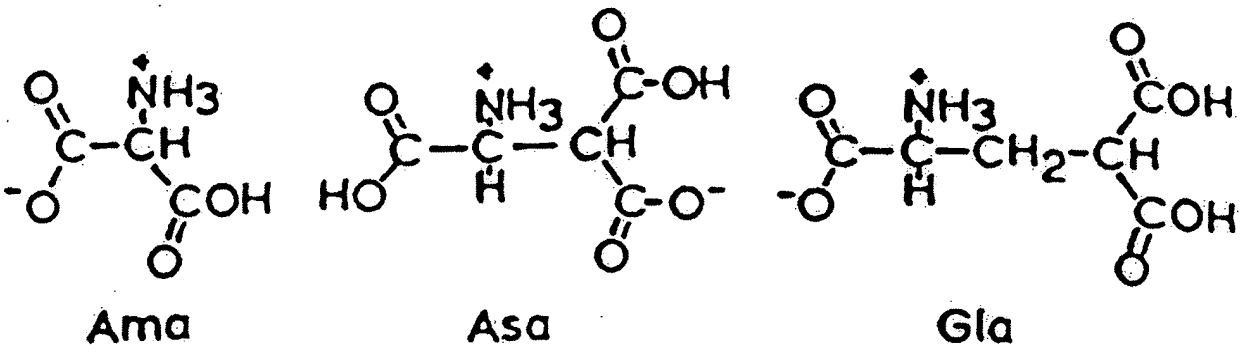

Figure 1. Ama (aminomalonic acid) and Asa (β-carboxyaspartate) were identified by anaerobic alkaline hydrolysis of E Coli and human atherosclerotic plaques and by gas chromatographic/mass spectral analysis. They represent examples of post-translational modifications analogous to GLA (γ-carboxyglutamate), a key amino acid in prothrombin.

Ama is a relatively unstable amino acid that is present in minor amounts in complex structures such as bacteria and tissues. Despite intensive work and external funding, Dr. Kirsch's laboratory was unable to determine the biological significance of Ama until Dr. Levine rediscovered the molecule in his studies of IRP-2 degradation and made contact with Dr. Kirsch. A lively collaboration and this BRP has ensued. Dr. Levine's interests center on the oxidative modification of proteins and their role in biologic processes. Dr. Levine's laboratory at the NIH (Section on Protein Function in Disease – Laboratory of Biochemistry) in collaboration with Dr. Tracey Rouault (Cell Biology and Metabolism Branch, Section on Human Iron Metabolism, National Institutes of Child Health and Human Development) has played a significant role in defining the key molecules and molecular mechanisms governing eukaryotic iron homeostasis. On the basis of a collaboration that began in the fall of 1999, Drs. Levine and Rouault have become consultants to Dr. Kirsch's project.

Dr Rouault and her colleagues in the course of studying the iron-dependent oxidation, ubiquitination, and degradation of iron regulatory protein-2 identified and characterized a 63 residue sequence within IRP-2 which was necessary and sufficient to render the entire protein sensitive to iron-dependent degradation (30). Collaborating with Dr. Levine, the NIH group demonstrated that degradation was initiated by iron-dependent oxidation of the protein, followed by its ubiquination, and then by proteosomal degradation. By both mass spectral and amino acid analysis, the oxidation was shown to be the conversion of one cysteine residue to aminomalonic acid. This oxidative modification may prove to be a signal for targeted protein degradation, thus an explanation for iron mediated IRP-2 degradation and the iron-sensing loop. Molecules tagged with this post-translational peptide modification have a short half-life, which explains their transient nature and accounts for our difficulty in obtaining reproducible analytic data. Dr. Kirsch's laboratory has prepared monoclonal antibodies to wild type IRP-2, wild type iron-sensing domain (63 amino acids), and a recombinant peptide from E Coli that contain the residues 138-200 from IRP-2. This peptide was prepared in Dr. Levine's laboratory. The sequence is shown below and has the 3 cysteine residues in **bold**. Efforts are ongoing to generate peptides corresponding to the 7 possible cysteine sequence permutations of the iron-sensing loop of IRP-2. Once these specific peptides are available mAb's will be generated for use in identification of the IRP-2 polymorphisms.

AIQNAPNPGGGDLQKAGKLSPLKVQPKKLP**C**RGQTT**C**RGS**C**DSGELGRNSGTFSSQIENTPIL

In conducting our assessment of IRP-2 in peripheral blood leukocytes of subjects with MCI we will use our standard anti-IRP-2 mAb's. An example of the immunofluorescent labeling technique is shown in **Figure 2**. In all our flow cytometry and immunofluorescent studies, a human embryonic kidney cell e (gift of Dr. Tracey Rouault) will be used as a positive control. These cells contain a plasmid insertion of the IRP-2 gene under the control of a tetracycline promoter. A quasi-negative control will be the non-tetracycline-induced cells, with lymphocytes from the "knock-out" mouse serving as the true negative control. In Dr. Green's laboratory we obtained the first confocal demonstration of IRP-2 in cells. Utilizing an immunofluorescence technique, identical to our proposed studies, wherein mAb to the IRP-2 wild type iron-sensing domain, conjugated to a green fluorescent marker (FITC), was used to label the fixed IRP-2 expressing and control cells **(Figure 2)**.

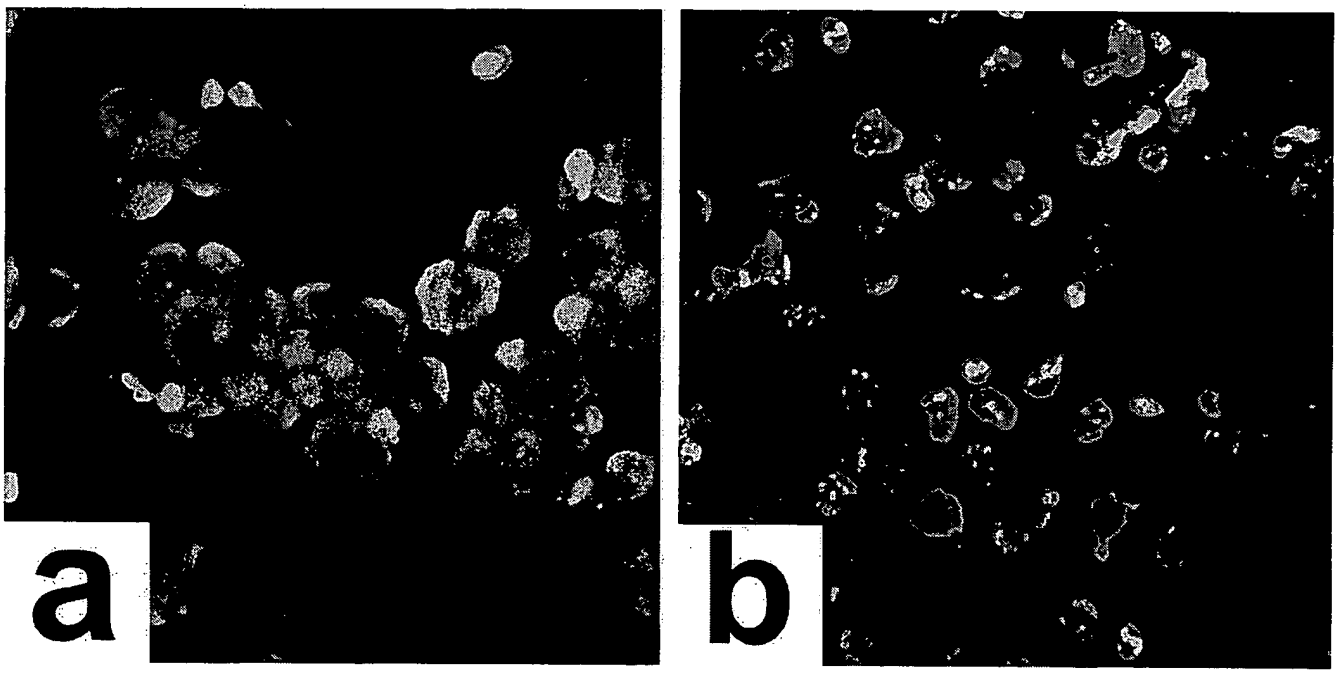

Figure 2. Confocal Image of Iron Regulatory Protein-2 Binding in Kidney Cells.

Panel a, shows the cytoplasmic binding of anti-IRP-2 (green) in the IRP-2 transfected kidney cells. The cell nuclei are counter-stained with propidium iodide (red). The control cells (non-tetracycline-induced) are shown in panel b. The control cells have a non-specific dotted immunofluorescence that appears to be localized predominantly in the nuclei of the cells. Magnification 40x.

A series of mAb's to IRP-2 and iron-regulated proteins, as well as, apoptotic markers and cytokine profiles in the MCI subject leukocytes will be conducted. As an example, preliminary studies were performed by Dr. Collins at BioErgonomics Inc. utilizing phycoerythrin and FITC labeled IRP-2 mAb's to detect intracellular IRP-2 protein in normal peripheral blood lymphocytes and human leukemic cell lines by flow cytometry. These initial studies demonstrated that IRP-2 is expressed only as an intracellular protein and that a small variable subpopulation of cells expressed low levels of IRP-2 in normal peripheral blood lymphocytes **(Figure 3 A and B)**.

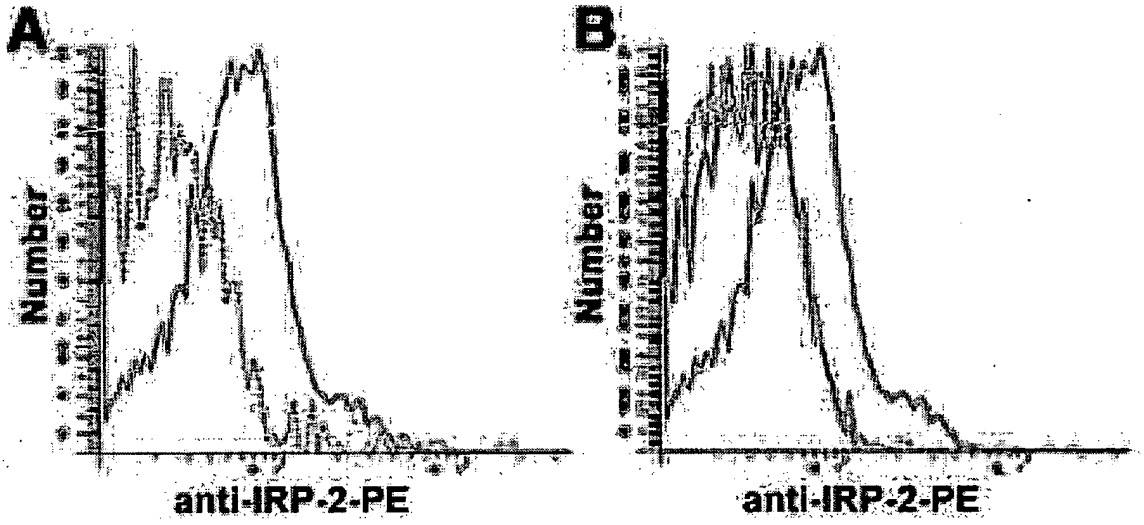

Figure 3. Expression of IRP-2 protein in Peripheral blood lymphocytes. In panel A the dotted line represents anti-IRP-2-PE staining of unpermeabilized cells (negative), the solid line represents anti-IRP-2-PE staining of permeabilized cells. In panel B the solid line represents anti-IRP-2-PE staining of permeabilized cells, the dashed line represents staining with an isotype control antibody and the dotted line represents staining of anti-IRP-2-PE antibody blocked by preincubation with unlabeled anti-IPR-2 antibody.

In continuously growing cell lines, like the KG-1 myeloid leukemia cell line, a much higher level of IRP-2 expression in a much higher percentage of cells was seen **(Figure 4).**

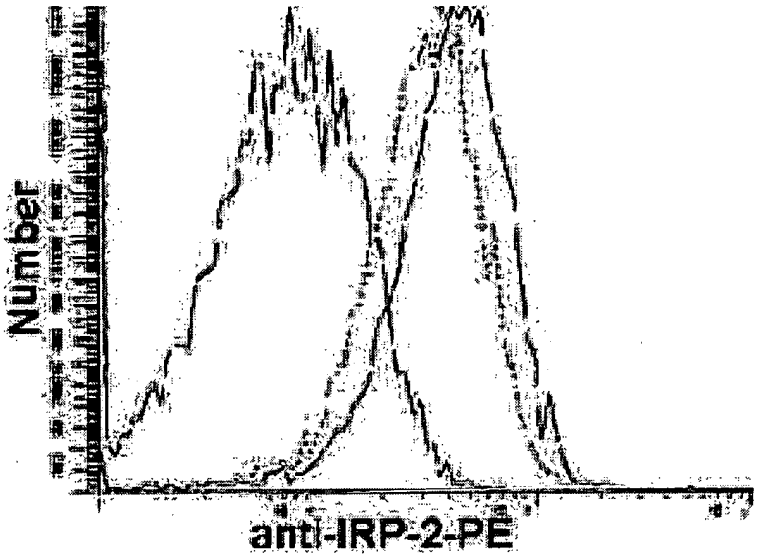

Figure 4. Expression of intracellular IRP-2 in the human AML cell line KG-1. Solid line represents staining with anti-IRP-2-PE, dashed line represents blocking by preincubation with unlabeled anti-IRP-2 antibody, Dotted line represents blocking with irrelevant antibody.

When expression of functional transferrin receptors was analyzed in conjunction with the IRP-2 molecule it was observed that the vast majority of these continuously growing cells co-expressed cell surface transferrin receptors and intracellular IRP-2 **(Figure 5).** AD lymphocytes labeled with anti-IRP-2 are seen in Figure 6.

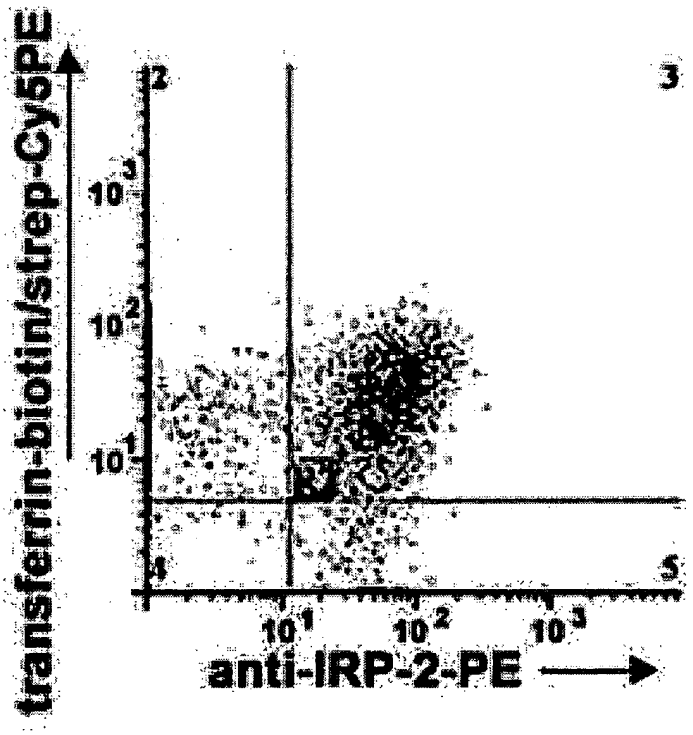

Figure 5. Co-expression of surface Transferrin receptors and intracellular IRP-2. Cells were labeled with biotinylated human transferrin and streptavidin-Cy5PE, then fixed and permeabilized and stained with anti-IRP-2-PE antibody. The vast majority of the cells were positive for both IRP-2 and cell surface transferrin receptors.

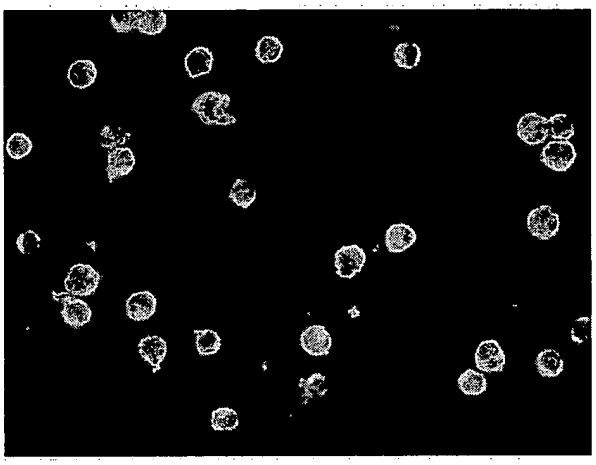

Figure 6. AD lymphocytes labeled with anti-IRP-2. An image of anti-IRP-PE labeled AD lymphocytes photographed at 100x magnification is shown. The fluorescent label is confined to the cytoplasm of the cells with no nuclear localization evident. This is the first visualization of IRP-2 protein expression in lymphocytes isolated from an AD patient, taken recently by Dr. Green.

The specifics regarding anti-IRP-2 iron degradation mAb's and our capabilities for generating mAb's utilized in our *ex vivo* studies (flow cytometry and fluorescent microscopy) are described in detail in Section D (Research Design and Methods).

The strategy for determining polymorphisms in IRP-2 is twofold. We will conduct an assessment of the nucleotide sequence of the iron-sensing domain obtained from RNA isolated from the peripheral blood leukocytes of the MCI subjects in our study. We will also test for protein modifications like Ama directly and by specific mAb's generated to various epitopes in the areas of the protein that are critical to iron sensing and degradation. The protein sequence of interest is amino acid 137 through 202 that corresponds to a 195-nucleotide sequence starting in the cDNA at nucleotide 411 through 606. Primers have been generated that will amplify this region in mRNA and using reverse transcriptase it can be made into DNA (RT-PCR). The DNA will be sequenced and compared to the known sequence. Sequencing the iron-sensing loop of IRP-2 in the lymphocyte RNA from our subjects should reveal whether this region is an area of polymorphic changes or subject to spontaneous mutation. Point deletions &/or substitutions can lead to frame shifts that result in defective protein products as we have seen for the tumor suppressor protein Cx32 (63). The specific details of these methods are in Section D (Research Design and Methods).

C.2.1. <u>Development of New MRI Technology to Quantify and Monitor Brain Iron in its Different *in vivo* States (aim 2).</u>

We conducted research in the area of gradient echo imaging and magnitude field effects on MRI signal loss and phase imaging for over fifteen years. Our work has been theoretical and experimental in nature, as well as clinical in practice. Working closely with Dr. Kido has resulted in several published papers during the last 8 years (64-66). Integrating four of our technical advances, should lead to absolute quantification of brain iron: high resolution 3D gradient echo imaging, phase imaging (SWI) with removal of background field effects, understanding T2* signal losses, and the extraction of susceptibility using a special spin echo/gradient echo imaging method.

C.2.2. High-resolution 3D, gradient echo imaging--- Obtaining sensitivity to small local field susceptibility effects requires imaging with long echo times. Background field effects caused by air/tissue interfaces lead to dramatic signal losses in tissues adjacent to these areas for long echo times. We previously demonstrated that dephasing across a voxel could be reduced by using very small voxels so that phase variation from background (or other) fields is reduced to less than 2π. This maneuver leads to a dramatic recovery of signal when images are filtered to recover the lost signal-to-noise. This results in higher resolution. The results are totally different than what would have been obtained with the lower resolution results. We refer to this as the commutator effect, i.e., a special non-linearity inherent in the

MR acquisition methods. We have imaged with echo times as long as 120 ms at 1.5T and shown that phase images represent a means to visualize susceptibility differences between tissues (52). Venous structures, gray matter/white matter susceptibility differences and iron in the basal ganglia become visible with this modification.

C.2.3. phase imaging and removing background field effects--- The use of phase images is a natural way to begin evaluating the presence of paramagnetic (or diamagnetic) differences between tissues in the brain. The phase in an MR image is given by $\varphi = \gamma \Delta B t$ where γ is the gyromagnetic ratio, ΔB the change in magnetic field from one tissue to the next, and t the time at which the data are measured (usually the echo time TE). The problem with visualizing these differences arises from the extra phase effects from a poorly shimmed field or background field effects from air/tissue interfaces which lead to aliasing of the phase information. We developed a high pass phase filter to remove these effects (67), made possible because the background field effects are predominantly low spatial frequency. Phase images dramatically improved with this processing technique (see **Figure 7**) and allow easy visualization of the basal ganglia in both normal and diseased states. This method has been successfully used to map oxygen saturation in the brain (68) and even small changes in oxygen saturation during functional brain activation. We can easily measure changes as small as 0.03 ppm with an error of 0.002 for the particular 3D sequence used for those experiments. This implies that, for a p value of 0.025, we can assert that susceptibility differences as small as 0.004 are measurable with this sequence. (The sequence used was a 5 minute, 3D gradient echo method with a TE = 40ms and a resolution of 0.5 x 1.0 x 2.0 mm^3). Sensitivity of the data can be improved if it is collected a second time and averaged, or by averaging multiple acquisitions as well as filtering the data to a lower resolution. (Figures 7, 8) Questions regarding optimal echo time to obtain optimal sensitivity remain open at this time.

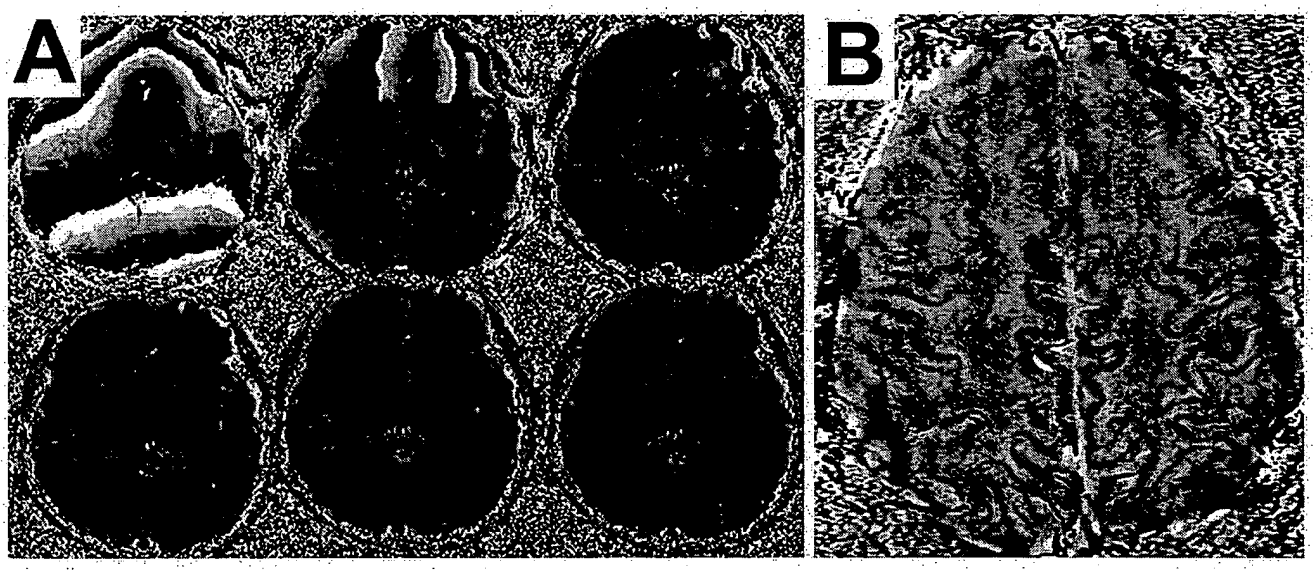

Figure 7. Panel A demonstrates our ability to display phase images (acquired at 1.5T with an echo time of 40ms and a resolution of $1mm^3$) without the usual bothersome aliasing artifacts that have heretofore rendered phase images of little utility. The image in panel B is a TE = 80ms image to show the phase difference due to iron between gray matter and white matter. The difference between the two is probably on the order of 1mg Fe/100 gm tissue. No other method we are aware of has the ability to be so specific and sensitive.

C.2.4. understanding T2* signal losses--- We continue to examine signal loss effects. Recently, we evaluated analytically the signal loss in a spherical voxel caused by a dipole field the source of which was a small volume enclosed within the voxel (67). Long echo times can induce significant oscillations

in the signal behavior (i.e., signal changes that are non-exponential in nature). In an attempt to quantify signal losses in T2* weighted imaging, we developed a theory that makes it possible to predict signal behavior in the presence of small randomly distributed local sources of susceptibility change. Specifically, we have shown that signal change is not exponential near the time origin and is exponential in the intermediate (and long) time domains. The theory can be used to extract the volume susceptibility of the random sources as well as their volume fraction within a voxel. The exact quantitative nature of this method has not yet been validated for a set of random structures *in vivo* but rather only via Monte Carlo approaches.

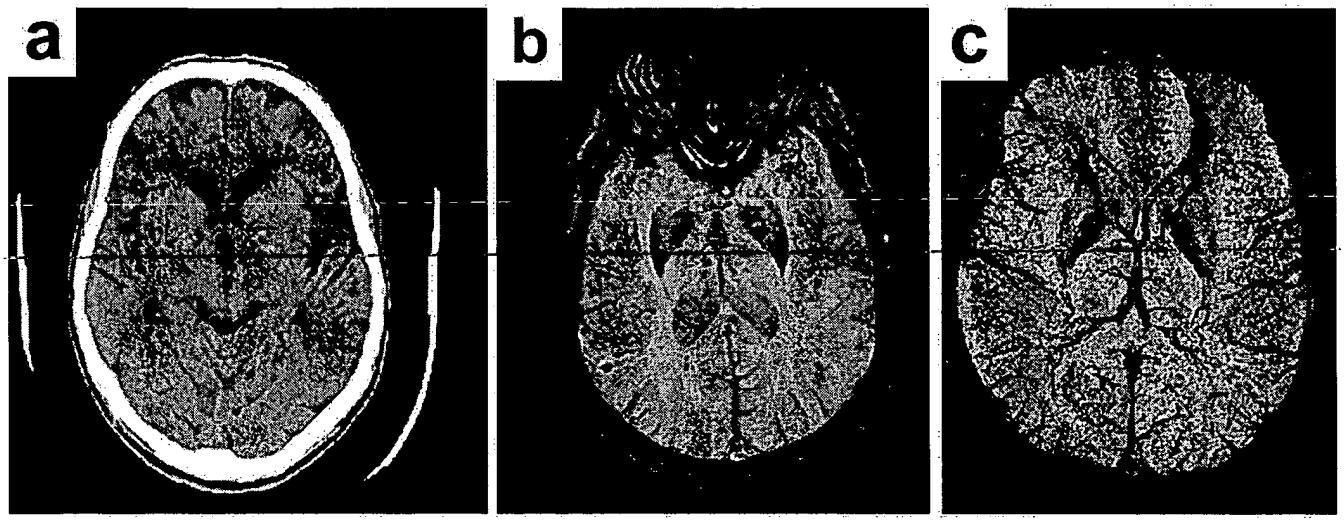

Figure 8. After the phase filtering is complete, the magnitude data itself can be highlighted using the phase image as a mask to enhance regions of susceptibility change such as those due to venous blood vessels and regions with increased iron content. The images in panel a and b are the CT image and the SWI image showing ferrocalcinosis. MR images are exquisitely sensitive to even small changes in local magnetic fields. Note how clearly the iron shows in the globus pallidus. The image in panel c shows both the venous vasculature and the increased iron in the globus pallidus and putamen of a healthy volunteer. No signs of abnormal iron or hemosiderin are present in this image.

We have also studied the dependence of T1 relaxation in the brain and found that frontal areas in the brain have the longest T1 for gray matter while areas near the motor cortex have the smallest T1 values. We noted that this causes a loss of contrast with gray matter and white matter in this region. We followed this up with phase measurements of the same regions and discovered a strong correlation between the two phases and hence iron showing the highest level in the motor cortex. We continued this work to show that the phase correlates strongly with iron content in the brain as a function of age (69).

C.2.5. extraction of susceptibility using a special spin echo/gradient echo imaging method--- In order to account for background field inhomogenities across a slice or voxel not caused by microscopic effects, and to eliminate any dependence on the rf pulse design as well, we designed a special combined gradient echo and spin echo acquisition method (52). A series of gradient echoes are collected around the spin echo and used to remove background field effects as follows. The last gradient echo is divided by the first gradient echo image to create the equivalent of a T2 weighted image without dephasing across the voxel. Once T2 is known, its effect on the multiple gradient echoes is removed so that only the pristine changes due to T2' (those signal changes caused by the local sources of susceptibility) remain. The signal dependence can be shown to have a quadratic behavior in time and, when fit, both the magnetic moment and volume content of the sources can be extracted quantitatively. This method will be discussed in more detail in the experimental design section.

Our MRI and flow cytometric studies will be validated with an experimental animal model (mouse) that has a targeted deletion of the IRP-2 gene, accumulates brain iron, and exhibits a progressive neurodegenerative disorder. Dr. Tracey Rouault and co-workers accomplished this engineered gene deletion (70).

C.3.1. The IRP-2 "Knockout" Mouse: Brain Iron Accumulation and Neurodegeneration

As noted previously, IRP's are cellular iron sensors and exert a post-transcriptional control over iron uptake, exit, and storage. Dr. Rouault has generated mice with a targeted deletion of the gene encoding IRP-2. Iron metabolism is disturbed in both the gut and the brain. As a consequence, the mice develop a neurodegenerative disease characterized by abnormal brain accumulations of ferric iron, ferritin, and ubiquitin position inclusions. These mice will serve as the model to validate both our new iron quantitating MRI sequences and *ex vivo* marker studies.

Steady state levels of iron in its various *in vivo* states (heme and non-heme, and in the latter category NTBI, TBI, ferritin) will be analyzed by quantitative histochemical techniques in the "knockout mouse," and correlated with MRI images to validate our new phase sequences.

Both Dr. Kirsch and Dr. Green have experience with quantitative immunohistochemical techniques and method development (71-74). Dr. Kirsch did two years of post-doctoral fellowship with Dr. O. Lowry, Washington University School of Medicine, and has published on these techniques. For example, he has conducted quantitative histochemical studies of the energy metabolism of the glioblastoma; measuring highly labile substrates of glycolysis in microdissected lyophilized tissue.

Dr. Kirsch has experience in microdissection, having spent a 6-week sabbatical in the Laboratory of Dr. Elaine Diamakakos at the Rockefeller Institute learning more advanced microdissection techniques. Quantitative analysis using Atomic Absorption Spectroscopy with Plasma Torch technology (Jet Propulsion Laboratories and/or West Coast Analytical, Santa Fe, CA) will be conducted on small tissue sections to quantify iron in its various states (NTBI, TBI, ferritin). These finding will be used to confirm the estimated iron content obtained with the MRI special sequences taken of the IRP-2 deleted mice, heterozygous and naïve mice. An example of the microdissection technique is shown in **Figure 9**.

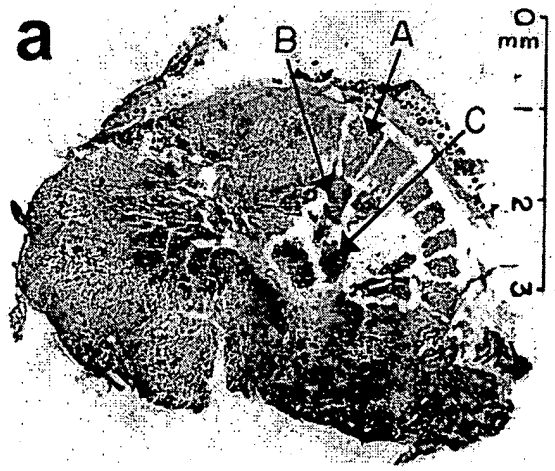

Figure 9. H&E Stained Glioblastoma Tissue.
The transverse frozen section of a mouse glioblastoma was dissected into zones indicated in image a and marked with an "A, B & C". These zones are shown magnified in the lower panels with zone A equivalent to image b, zone B equivalent to panel c and zone C represented by image d. This micro-dissection technique will be used to isolate areas of the knockout mouse brain tissue to quantify brain iron.

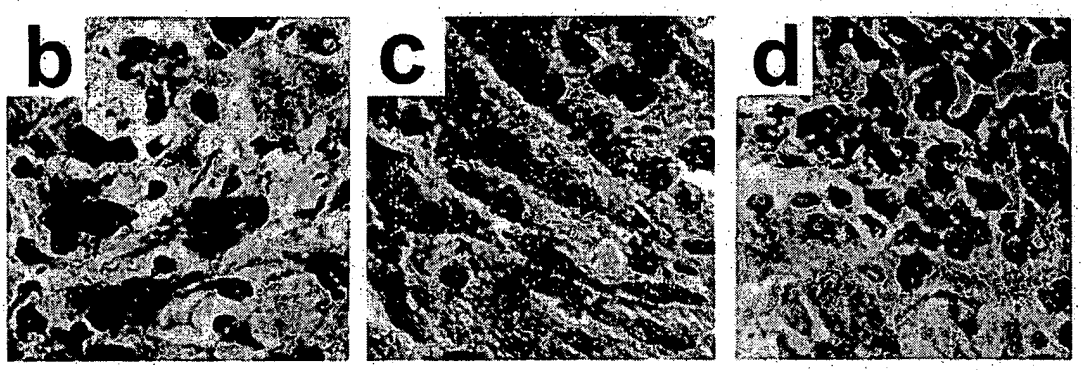

Immunohistochemical examination of the mouse brain tissue will be performed in Dr Green's laboratory using fluorescent imaging (laser scanning cytometery and confocal microscopy). An example of a fluorescent map of a rat brain slice with a red nuclear fluorescent label is shown in **Figure 10.**

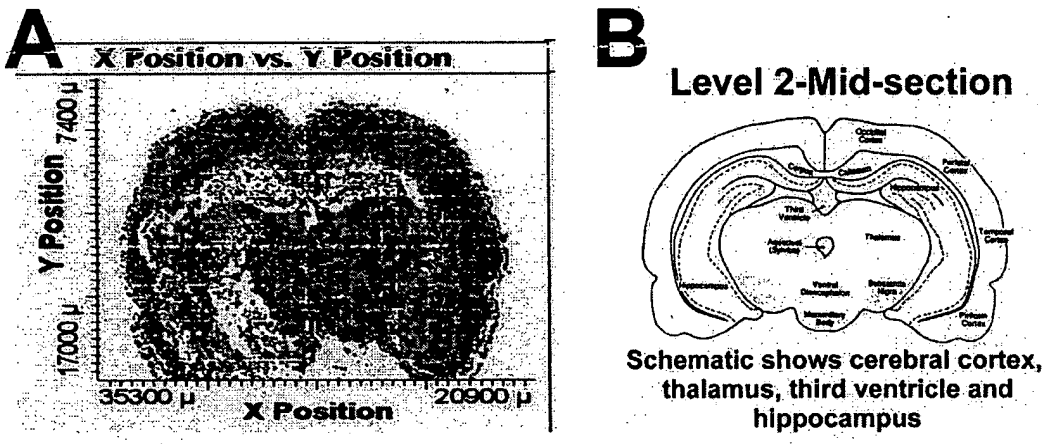

Figure 10. Laser Scanning Cytometric Map of Rodent Brain Tissue. Panel A, shows an example of a fluorescent map of a rat brain tissue section labeled with propidium iodide which stains all cell nuclei red. As the laser scans (0.5µm) through the section each cellular event is assigned an x, y coordinate and placed in a designated window, when the scan is complete a 2-dimensional map is generated that shows general section morphology. When additional immuno-fluorescent markers are employed their color will be displayed where they localize within the tissue. This methodology is used in the immuno-histochemistry section of this proposal. Panel B, for comparison, depicts the structures present in the mid-brain similar to those defined in the fluorescent map.

C.3.2. Clinical Applications of *ex vivo* Marker Tests and MRI Studies to a Subject "a" Diagnosis of Mild Cognitive Disorders (aim 3)

A team consisting of Drs. James Larsen, Wolff M. Kirsch, Daniel Kido, William Britt, Daniel Collins and Floyd Petersen will conduct the clinical applications of the minimal invasive technological and psychometric studies. Each member of the team has expertise and a clinical background to enable accomplishment of the proposed tasks.

The proposed subject population will be drawn primarily from the gerontology practice of Dr. James Larsen who is the medical director of four different long-term care facilities in the Loma Linda area. He has been in full time academic practice here at LLU, sees from 6-8 MCI patients per month in his clinics, and follows his patients from initial introduction to death. He has excellent longitudinal follow-up in all of his cases, and has noted upwards of 15% of his MCI patients to progress to an accelerated dementing course over a year. Dr. Britt performs psychometric tests on a number of his cases. Dr.

Kirsch is an active neurosurgeon with a special interest in the surgically treatable elderly dementias. He currently follows in his clinic 42 elderly patients with "Normal Pressure Hydrocephalus" (NPH). He has devised a minimally invasive procedure to treat NPH (59). Dr. Kirsch has worked with Dr. Britt in evaluating his NPH cases in longitudinal follow-up. Dr. Collins is an immunologist with extensive expertise in flow cytometry, development of novel techniques and reagents, and cytokine biology. He will aid in the interpretation of flow cytometric data and correlation of *ex vivo* blood tests and clinical course.

D. RESEARCH DESIGN AND METHODS

D.1. Description Page

The institution directing this Bioengineering Research Partnership is the Loma Linda University (Neurosurgery Center for Research, Training and Education, Departments of Molecular Biology and Molecular Genetics, Biochemistry, Radiology, Radiobiology, Internal Medicine, Psychiatry and Pathology). Partners include BioErgonomics Inc., St Paul, MN and the MRI Institute for Biomedical Research, St. Louis, MO. The goal of our multidisciplinary partnership is to define the role of altered brain iron metabolism as a risk factor for Alzheimer's Disease in the context of elderly MCI patients. The engineering focus of the study is: (1) defining *ex vivo* markers in peripheral blood cells indicating iron or amyloid perturbations and (2) the development of a new magnetic resonance imaging (MRI) technology to quantitate and differentiate brain iron. Study subjects will be 75 patients (50 years of age or older) with mild cognitive impairment who will be followed longitudinally for a three to four year period with sequential psychometric tests, special MRI sequences, and peripheral blood cell studies. Control subjects will consist of 25 healthy age-matched individuals who will be subjected to the same tests as the MCI group. A genetically engineered mouse with an iron regulatory protein 2 "knockout" that accumulates abnormal quantities of brain iron and displays a neurodegenerative disorder will be used to validate our new technology. A search for polymorphisms in the IRP-2 gene will be part of each patient's evaluation. At four years of serial follow-up it is anticipated that about 50% of the 100 study subjects will have AD, and correlations of psychometric data, brain iron localization and quantitation, as well as immunocytochemical peripheral blood will be established using statistical consultation and autopsy information if available.

TABLE D.1. MILESTONES FOR EACH YEAR

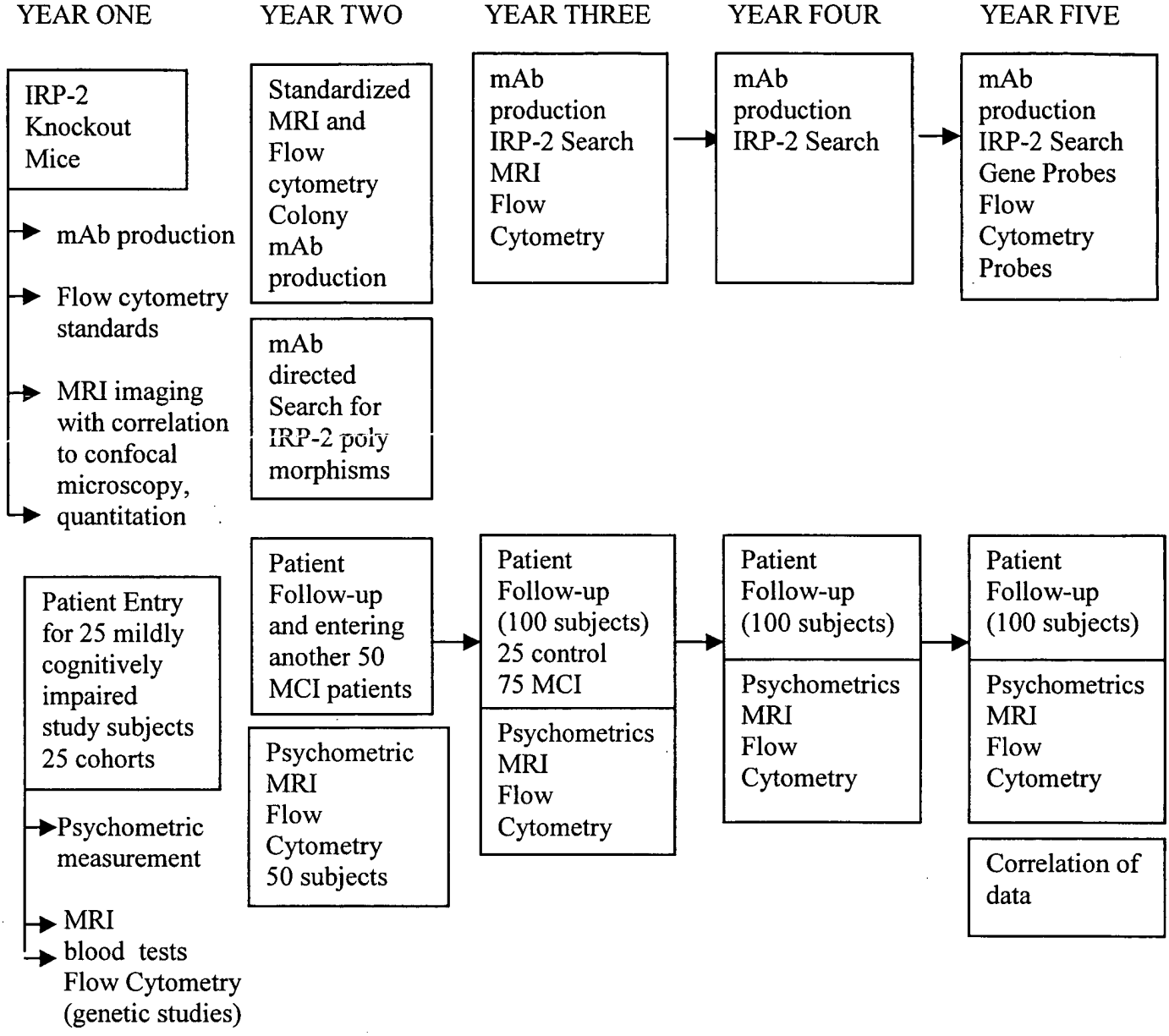

SPECIFIC AIMS					
1	X	X	X		
2	X	X	X		
3	X	X	X	X	X

TABLE D.2. ORGANIZATION CHART

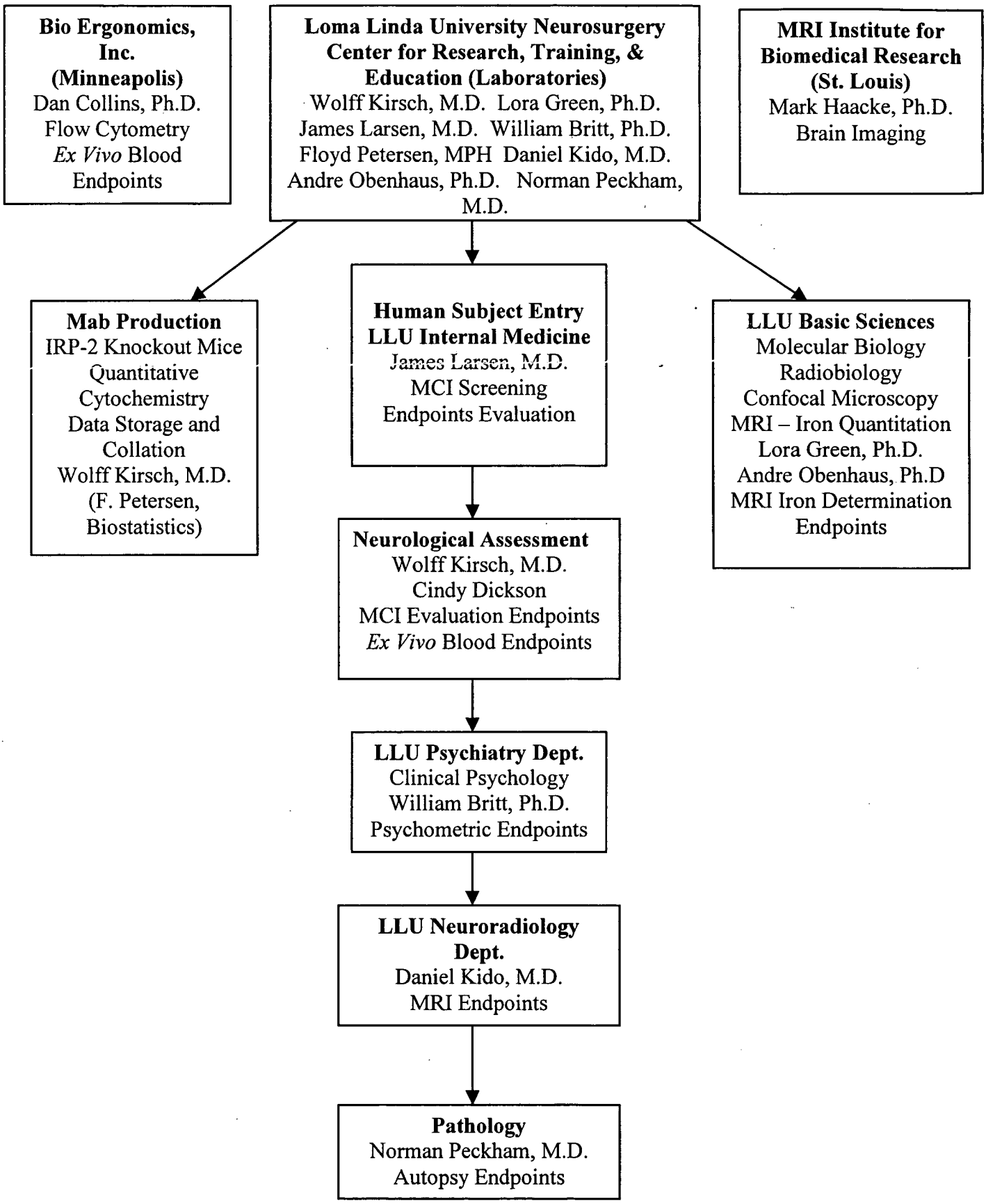

D.2.1. Evaluation and Assignment of Subjects

We plan to set up "outreach" programs in nearby cachement areas that have large elderly populations in order to selectively recruit cases. (Hemet, Palm Springs, Riverside, San Bernardino). Special attention will be directed to enroll cases from our large Hispanic and Oriental populations. Women and members of minority groups as well as their subpopulations will be included in the enrollment.

On the basis of a review of Dr. Larsen's statistics we can plan to enroll 25 MCI cases and 25 age matched controls in the first year of the study from his referral and cachement base. Our plan is to enroll an additional 50 MCI subjects in the second year of the study. As noted, our preliminary studies have generated interest by "word-of-mouth" publicity and prospective patients have been calling Dr. Kirsch's office for a "free evaluation." We will advise local internists and neurologists of our BRP, which will be clearly defined as research with no clinical care offered or provided.

Dr. Kirsch will then screen subjects referred by Dr. Larsen or identified by self-referral in his weekly clinic. Dr. Kirsch specializes in the surgical treatment of elderly "Normal Pressure Hydrocephalus" and will use this evaluation to conduct a preliminary screen to differentiate the diagnosis of MCI. Subjects who have normal global cognitive function but signs of memory impairment without dementia or history of a major neurological or hematological disorder will be then referred to Dr. Britt for a more detailed psychometric evaluation to qualify for enrollment.

The following criteria must be met in order to be entered as an MCI subject in this study. Additional screening will be done by Dr. Britt after referral by Dr. Kirsch for patients who meet the following criteria.

1) Age > 50 years
2) Education > 7^{th} grade
3) No history of major neurological, hematologic or iron metabolic disorder
4) No history of substance abuse (alcohol, narcotics)
5) Memory complaints by patient, family or physician
6) Normal global cognitive function (MMSE – minimental state examination ≥ 10)
7) Objective memory impairment or impairment in one other area of cognitive function as evidenced by a score > 1.5 SD's (standard deviation) below the age appropriate mean
8) No dementia
9) Able to give informed consent

Guidelines and predictive recommendations for the early detection of MCI in the elderly have recently been published (56, 57, 60, 61) and will be followed explicitly in our study. Dr. Britt will confirm the diagnosis by a repeat examination evaluating the following criteria:

1) Memory complaint by patient, family or physician.
2) Normal activities of daily living (CDR score of 0.5).
3) Normal global cognitive function (MMSE>10).
4) Objective memory impairment or impairment in one other area of cognitive function as evidenced by score > 1.5 SD's below age appropriate mean.
5) Not demented.

The results of the general physical, neurological, radiological, and psychometric evaluation on each subject will be discussed by Drs. Larsen, Kirsch, Kido, Britt and Mr. Petersen before enrolling any subject in the program. This screening will be selective in order to homogenize our MCI cohorts. The "flow diagram for subject study is given in Table D.2.2.

Table D.2.2.

Flow Diagram of MCI Subject Entry in the Study

Initial Evaluation – Dr. James Larsen
Referred because of memory disturbance

↓

Neurological assessment: Dr. Wolff Kirsch
Differential diagnosis (for example, - Normal Pressure Hydrocephalus, Multifunctional Dementia)

↓

Psychometric assessment: Dr. Britt
Establish Diagnosis of MCI or Control
MMSE ∃ 10
Activities of daily living
CDR score 0.5
Objective memory impaired
An impairment in other areas of cognitive function
Score < 1.5 S.D.'s below age appropriate mean
Not demented

↓

Enrolled in BRP Research (Continue to see Drs. Kirsch and Larsen every 6 months)
MCI cohort n=75
Control cohort n=25

↓

Dr. Larsen – Blood Drawing 2 x per year

↓

Dr. Kido – MRI 1 x per year

↓

Dr. Britt – Psychometrics 1X per year (Section D.2.3.)

↙ ↘

conversion rate 6-25%/year ( )
(Dr. Larsen's Experience 15%/year)
more advanced deterioration
accelerate MRI, psychometric evaluation and blood evaluation
autopsy (if allowed)

start on 3-4 year period follow-up
Studies as noted above

D.2.3. Psychometric Evaluation After Enrollment as an MCI Subject or Control:

In keeping with the intent of this proposal to study subjects who have MCI we will exercise critical control of the enrollment process. A panel of tests will be administered with proven diagnostic value for preclinical and clinical AD . The rate of conversion to AD has been estimated between 6 and 25% per year for MCI (56). Neuropsychological tests and ADL rating scales will be done which detect impairment in verbal delayed recall, set switching, planning and organization, and cognitively demanding ADL's.

Verbal memory tasks known to detect loss of information over delay in elderly presymptomatic subjects typically measure word list learning, paired associate learning and more complex recall of stories (75, 76). Subtests of the Wechsler Memory Scale III that measure these domains will be used in this study. In the case of the WMS-III, a scoring computer program developed by the test publisher (Psychological Corp.) will be used to score the tests (77).

Two measures of executive functioning that capture set shifting and planning and organization are the Wisconsin Card Sorting Test and Trailmaking Test B. Both are widely used clinically and in research studies for AD will be applied (75).

In order to assess more complex ADL's, the Clinical Dementia Rating (CDR) is recommended for its ability to measure orientation, judgment, memory, community affairs, personal care, and home and hobbies (56, 78).

It is often difficult to determine whether the subject has become depressed in recognition of cognitive and functional decline or whether the depression came first, resulting in pseudodementia. The Mini Mental Status Examination can assess not only depression but global cognitive functioning. Depression is typically more common in early stages of AD when the subject begins to experience memory problems, but the incidence of a major depressive disorder is estimated to be low (79).

Psychometric studies will be routinely done once per year (3 sessions of one to two hours) for every subject. If an accelerated cognitive deterioration is noted tests will be performed more frequently. The results of the psychometric evaluation will be reviewed by Drs. Larsen, Kirsch, Britt and Mr. Petersen every 2 weeks. Frequency of evaluations will be based on the clinical course of individual subjects.

A close relationship will be established between the subject population and the caring physicians and psychologists. Drs. Larsen and Kirsch already have this relationship with cognitively affected subjects at present. For example, Dr. Kirsch follows closely the clinical course of over 40 elderly patients with "Normal Pressure Hydrocephalus" that have received his new minimally invasive procedure for the treatment of adult hydrocephalus. Dr. Larsen has an identical this relationship with his MCI and AD patients. His approximate conversion rate of MCI cases to AD is about 10-15%/year. MCI subjects will be followed with no restrictions on their therapy or nutritional supplements. Their clinical course will mandate the repetition of psychometric, blood or MRI tests. A rapport will be established with the family members in order to gain access to age-matched "normal" controls will to enroll in the study. In the event of death, an effort will be made to obtain an autopsy and permission to examine the brain. Dr. Norman Peckham, a board certified neuropathologist, will conduct the brain post- mortem examination according to guidelines established by CERAD (80).

The clinical members of the BRP as well as Dr. Collins will meet once per week for a 2 hour period to discuss and evaluate results of each subject. Mr. Floyd Petersen, our biostatistician, will attend each meeting. Each subject will have dossier with critical parameters recorded. Subjects with an accelerated

dementing course under observation will have more frequent evaluations to document blood, psychometric, and MRI changes. The subjects will have special assays of peripheral blood to seek polymorphisms of circulating IRP-2 and alteration iron homeostatic events in peripheral lymphocytes.

D.3.1.1. Specific Aim #1: Define *ex vivo* markers for AD in peripheral blood leukocytes of MCI and control subjects by flow cytometric, immunocytochemical identification of the iron sensing peptide domain of iron regulatory protein-2 (IRP-2), amyloid precursor protein (APP), spontaneous and stimulated apoptosis, and cytokine expression by multiplexed flow cytometric analysis. Identify IRP-2 polymorphisms in the iron-sensing loop of the IRP-2 gene using RT-PCR and posttranslational modification of IRP-2 protein using monoclonal antibodies.

D.3.1.2. Location of Work: LLU and BioErgonomics Inc. (St. Paul, MN).

D.3.1.3. Experimental Design: Volunteers in the study will be segregated into the MCI group or the age-matched cohort group according to the psychological evaluation criteria defined in the previous section. We anticipate 25 subjects to be enrolled in each study group during the first year and an additional 50 MCI patients to be enrolled in the second year. Peripheral blood samples will be obtained from MCI patients in both Dr. Larsen's and Dr. Kirsch's clinics, collated and coded prior to delivery for analysis. Twice per year, each subject in the study will have 20-30 ml of peripheral blood collected into heparin anti-coagulated vacutainer tubes. Ten ml of blood will be directed to Dr. Green's laboratory for polymorphism studies, the remainder of the blood will be sent to Dr. Collins' laboratory at BioErgonomics Inc. for tissue culture and analysis of cell surface βAPP on peripheral blood leukocytes, expression of intracellular IRP-2, spontaneous and stimulated expression of proinflammatory cytokines, and spontaneous and stimulated apoptosis. Accelerated collection of blood samples will ensue in the MCI subjects that show obvious clinical deterioration.

D.3.1.4. Key Endpoints:

- IRP-2 and transferrin receptor identification and quantification in peripheral blood leukocytes
- APP expression in peripheral monocytes and platelets
- Proinflammatory cytokine expression in peripheral monocytes
- Apoptosis in peripheral lymphocytes
- Identification of IRP-2 polymorphisms

D.3.1.5. Specific Methods

D.3.1.5.1. Preparation of Leukocytes and Flow Cytometric Studies

Mononuclear cells are prepared from heparin anticoagulated peripheral blood samples by density gradient separations using 68% Percoll. Briefly, 20 ml of undiluted whole blood samples are layered onto 25 ml of 68% Percoll in a 50 ml centrifuge tube. The blood is then centrifuged for 20 minutes at 800 x g. The interface cells will be collected and pelleted by centrifugation. The cell pellet will be disrupted by vortexing and the remnant erythrocytes are removed by lysis using 25 ml of VitaLyse erythrocyte lysing buffer (BioErgonomics Inc.). Cells are washed once with 25 ml of PBS and then resuspended to 1 x 10^7 mononuclear cells/ml. One hundred microliters of cells (1 x 10^6) are used for each labeling procedure.

For stimulation of inflammatory cytokine expression, cells will be resuspended in either Basal Medium or ActiCyte-LPS medium (BioErgonomics Inc. St. Paul, MN) at a concentration of 1 x 10^6 cells/ml and incubated for 20 hours at 37°C in an atmosphere of 5% CO_2. During the last 4 hours of incubation, the Golgi inhibitor Brefeldin A (10 ng/ml) will be added to the cultures to inhibit the secretion of cytokine

and enhance the intracellular staining. After the incubation period, cells will be harvested and the culture supernatants will be retained for cytokine secretion analysis and the cells will be retained for detection of intracellular cytokines.

Activation of lymphocytes for the detection of altered levels of intracellular IRP-2 protein or induction of apoptosis will be performed in the following manner. One million mononuclear cells will be resuspended in either Basal Medium or ActiCyte-TC medium (BioErgonomics Inc., St. Paul, MN) and incubated for 48-72 hours at 37°C in an atmosphere of 5% CO_2. ActiCyte-TC medium contains anti-CD3 antibody and the human cytokines Interleukin-1 alpha (IL-1α) and Interleukin-2 (IL-2). This medium specifically activates T-lymphocytes via the epsilon chain of the T-cell antigen receptor and the receptors for the two cytokines.

D.3.1.5.2. Fluorochrome Labeling of Antibodies

To label antibodies with FITC, antibodies are exchanged into 100 mM KH_2CO_3 buffer (pH 9.0) at a concentration of 5 mg/ml. FITC (Molecular Probes) (10 mg/ml in DMF) is added to the antibody at a 25:1 molar ratio and incubated for 1 hour at room temperature, in the dark. Free FITC is separated from the antibody on a G-25 Sephadex column. Phycoerythrin and Cy5PE conjugates are produced using 2-iminothiolane to modify the fluorochrome and sulfo-SMCC to modify the antibody. The modified proteins are then incubated together for 1 hour at room temperature in the dark. Free fluorochrome and antibody is separated from fluorochrome-conjugated antibody by separation on Sephacryl S-300-HR columns (Sigma). Alterations in the ratio of fluorochrome to protein may be necessary to optimize the fluorescent signal for a particular antibody or peptide antigen.

D.3.1.5.3. Quality Control of anti-IRP-2 Antibody development and Fluorochrome Labeling

The antibodies that are developed against the IRP-2 native, mutant peptides and intact proteins will be tested for specificity using both antigen-down ELISA and a micro particle–based immunofluorescent assay developed at BioErgonomics Inc. When available, biotin-labeled native and mutant peptides or intact IRP-2 proteins will be attached to 7 μm diameter avidin-coated polystyrene paramagnetic particles that bind, with high specificity and avidity, biotin-labeled molecules. The newly developed antibodies will be tested for specificity against the micro particles coated with the individual various IRP-2 peptides by sandwich assay. IRP-2-specific antibody bound to the antigen-coated particles will be detected by subsequent reaction with phycoerythrin-labeled goat anti-mouse Ig antibody. Samples will be analyzed by flow cytometry. Antibodies that produce a positive fluorescence signal will be considered potentially specific for the native or mutant peptides. Specificity will be confirmed by blockade of specific binding and fluorescence of anti-IRP-2 antibody by pre-incubation of cells or antigen-coated particles with the same unlabeled antibody or pre-incubation of labeled antibody with antigen prior to incubation with the cell or antigen-coated microparticle.

Antigen-coated microparticles will also be used for quality control of the fluorescent conjugation of the previously selected IRP-2 specific antibodies. Optimal labeling of the anti-IRP-2 antibodies with either phycoerythrin or Cy5-phycoerythrin fluorescent dyes which produce optimal signal-to-noise ratios will be selected based on binding to antigen-coated microparticles and intracellular labeling of both antigen-positive and antigen-negative cells populations. Grouping of specificities of antibodies for particular epitopes of the IRP-2 peptides or complete molecules will be determined by specific blockade of fluorochrome-labeled antibodies with unlabeled antibodies.

D.3.1.5.4. Expression of Surface Membrane forms of βAPP

The relative expression of cell surface membrane forms of βAPP will be determined for study subjects by flow cytometric analysis. Briefly, isolated mononuclear cells will be stained with the monoclonal antibody 22C11, which is specific for the n-terminus of the βAPP (Boehringer Mannheim) for 30 minutes and phycoerythrin-conjugated CD14. After incubation with the antibodies, cells will be washed once with PBS to remove unbound antibody and the cells will then be analyzed by flow cytometry.

D.3.1.5.5. Expression of Functional Cell Surface Tranferrin Receptors

The relative expression of functional transferrin receptors on cells from test subjects will be determined by flow cytometric analysis. Briefly, isolated mononuclear cells will be stained with 100 ng of phycoerythrin-conjugated human tranferrin (BioErgonomics Inc.) for 15 minutes and washed once with PBS to remove unbound conjugate prior to flow cytometric analysis. Expression of functional receptors (that is, receptors actually capable of binding transferrin) is directly proportional to the intensity of fluorescence of the cells.

D.3.1.5.6. Intracellular Labeling of Cells with Fluorochrome-labeled anti-IRP-2 antibodies

Expression of intracellular IRP-2 loop peptide has been determined by flow cytometric analysis using FITC, PE and Cy5PE-conjugated anti-IRP-2 monoclonal antibodies to identify cells expressing the native IRP-2 proteins. Experiments are projected to search for IRP-2 iron degradation domain polymorphisms. Washed cells (1×10^6 in 100 µl of PBS) are fixed by incubation in 1 ml of 1% formaldehyde for 30 minutes for expression by specific binding of fluorescently labeled antibodies directed against intracellular IRP-2 proteins. Positive fluorescence and identification of specificity for a particular anti-IRP-2 antibody will be determined by a shift in fluorescence intensity that can be specifically completed by preincubation with antigen or unlabeled antibody. Cells positive for a particular anti-CD antibody will be determined by a comparison to similarly-labeled isotypic control antibody or cells whose fluorescent staining was specifically-blocked by unlabeled antibody.

D.3.1.5.7. Expression of Proinflammatory Cytokines by Circulating Leukocytes

Mononuclear cells (1×10^6/ml) will be incubated for 20 hours in the presence or absence of bacterial lipopolysaccharide (LPS) to determine basal and stimulated production of the proinflammatory cytokines Interleukin-1 alpha (IL-1α), Interleukin-6 (IL-6), and Tumor Necrosis Factor-alpha (TNF-α). Identification of cytokine producing cells will be performed by flow cytometry analysis of intracellular cytokines. Briefly, cells will be fixed and permeabilized as described for the identification of IRP-2 proteins. The cells will then be labeled with PE- or Cy5PE-labeled antibodies specific for IL-1α, IL-6 and TNF-α. The amount of cytokine secreted into the culture media during the 20-hour incubation will be measured by a flow cytometric-based quantitative immunofluorescent assay (ImmunoFlow and MultiFlow, BioErgonomics Inc., St Paul, MN).

D.3.1.5.8. Detection of Apoptosis or Necrosis in Activated Mononuclear Cells

Briefly, one million mononuclear cells activated by ActiCyte-TC (containing anti-CD3, hIL-2, hIL-1 alpha) will be washed with PBS and stained with the phosphatidylserine binding protein Annexin-V-FITC (200 ng, Caltag, South San Francisco, CA) and the DNA-intercalating dye Propidium Iodide (4

ug) in the presence of Ca^{+2} containing annexin-V binding buffer. Cells that are positive for Annexin-V alone or Annexin-V and Propidium Iodide are considered as early or late-stage apoptotic, respectively, while cells that are positive for Propidium iodide alone are considered necrotic.

D.3.1.5.9. Preparation of Leukocytes for RT-PCR

Mononuclear cells will be separated from 10 mls of whole blood similar to that described above for flow cytometry. The isolated leukocytes will be resuspended in 1 ml of TRIzol® Reagent (Life Technologies Cat# 15596.) per 5 x 10^6 cells. The RNA will be extracted using standard methods like that described in Green *et al.* 1995 (81).

D.3.1.5.10. RT-PCR of IRP-2 Iron-Sensing Loop in Human Leukocytes

The RNA isolated from human subject leukocytes will be used in a standard two-step RT-PCR reaction using ProSTAR™ Ultra HF RT-PCR System (Stratagene Cat#600166.) The sequence of interest was derived from the published cDNA accession # p48200, with nucleotide sequence 411 to 606 corresponding to the portion of the protein that contains the 3 cysteines and forms the iron-sensing domain. Primers for this iron-binding region of the IRP-2 gene were selected using the Web Primer software provided by Stanford University (http://genome-www2.stanford.edu/cgi-bin/SGD/web-primer.) With the optimum primers being:

5' TGCAGAAAGCAGGAAAGCT and 3' GGCACTGGTTGCAAATGAA

The RT-PCR reaction will be performed in a MJ PTC-220 Themocycler. The reverse transcription will be done with Oligo (dT) primer and StrataScriptRT for 30 minutes at 42°C. The PCR steps will be set up according to the kit recommendation with an annealing temperature of 50°C for 1 minute for 40 cycles. Once the RT-PCR products are produced they will be run on low melting-point agarose gels.
The designated bands from the RT-PCR gels will be cut and purified using Qiaex II Gel Extraction Kit (Qiagen, Valencia, CA) (63, 82). The cut bands will be melted in a mixture of 400µl of QX1 buffer and 15µl Qiaex II beads at 50°C for 15 min. After centrifugation at 14,000 rpm for 30s, the pellets washed once in QX1 buffer to remove any remaining agarose, then twice to remove residual salt contaminants. After air-drying for 2 hrs at room temperature, the pellets will be eluted in 10mM Tris and the DNA supernatants sent to the Center of Molecular Biology and Gene Therapy (Loma Linda University) for sequencing.

BLAST Alignment: To determine if the RT-PCR products from the MCI subjects corresponds to the expected region of the IRP-2 gene, the resulting DNA sequences will be aligned with the known human sequence database from the National Center for Biotechnology Information web site (www.ncbi.nlm.gov). This alignment uses the BLAST (Basic Local Alignment Search Tool) program.

D.3.1.5.11. Expected Results and Alternatives

It is anticipated that missregulation of iron will have an important contributory role in the development of pathology and severity of disease in the transition of patients from the MCI classification to AD. This could be due to missregulation of the IRP-2 molecule by a number of possible mechanisms. We will have obtained sequence information on the iron-sensing domain of IRP-2, which also serves as the ubiquination site for proteosome-mediated degradation. There are now several examples of spontaneously arising mutations in tumor suppressor genes like p53 and Cx32 (83, 84). These mutations are often point deletions that cause a frame-shift that can prematurely stop protein translation or cause significant alteration in the resulting protein so that it is non-functional. If spontaneous polymorphisms

arise in the MCI to AD subjects this modification will clearly explain the observed abnormalities in iron metabolisms and processing. If the gene product is not altered in these subjects relative to the healthy cohort we will pursue altered post-translational modifications critical to iron regulation. As the specific mAb's to the permutations of the 3 critical cysteines become available (from Drs. Kirsch & Levine) they will be employed in the future analysis of IRP-2 expression and function. These could include overexpression of normal functional IRP-2, inhibition of ubiquitination and destruction of the protein in the proteosome, malfunction of the proteosome secondary to overproduction of Aβ, or polymorphisms of the IRP-2 molecule encoding oxidation resistant degradation domains resulting in reduced ubiquitination. If there is evidence of oxidation resistant degradation domains in the IRP-2 molecule, isolation and sequencing of this domain would enable creation of complementary nucleic acid sequences and the development of specific probes to detect the presence of mutant IRP-2. Overproduction of normal IRP-2 would suggest looking in the promotor regions for mechanisms of regulation. If it appears that correlation of a number of these different measurements are necessary to differentiate AD from other pathologies, that information could become the basis for the development of kits which could aid in the processing of and analysis of blood samples for the appropriate criteria. This approach raises the possibility of defining *ex vivo* markers for AD as well as establishing criteria for evaluating potential gene therapies.

D.4.1.1. Specific Aim #2: Develop new magnetic resonance imaging (MRI) technology for quantification and monitoring of brain iron in it's various *in vivo* states (non-transferrin bound iron-NTBI, transferrin bound iron-TBI, and high molecular weight complexes – ferritin, hemosiderin). Validate the findings using an experimental mouse model with an engineered deletion of IRP-2 that accumulates brain iron and develops a neurodegenerative disorder.

D.4.1.2. Experimental Design:

This aim has both clinical and experimental aspects. With regard to the clinical, MCI patients selected for entry into the study will have, following the other tests and evaluations, an MRI performed. The MRI will be analyzed using special sequences that have been developed by Dr. Haacke (MRI Institute, St. Louis, MO) under the supervision of Dr. Daniel Kido (LLU)(67, 68). The results of these tests, and original images, will be stored and correlated with perturbations in iron metabolism, detected in fluorescence based assays of IRP-2 (aim 1). These findings will be correlated longitudinally with the natural history of the cases through sequential examinations. To improve and validate the MRI iron quantification a transgenic mouse that accumulates brain iron will be studied. Improvements made to the imaging technology will be applied to the MCI subject MRI's thereby advancing our ability to non-invasively image and possibly detect iron changes that correlate with clinically escalating dementia.

A new approach to brain imaging referred to as ***SWI (susceptibility weighted imaging)*** is our strategy to quantify brain iron content. This approach suggests that using local phase differences to map iron will allow predictions to validate results from the previous static dephasing regime approaches. We have shown that phase and iron content correlate with age (69). It is currently difficult to demonstrate this with standard T2 because reversibility effects occur in both Parkinson's disease and AD, which nullify the usual effects of iron. However, phase and T2 prime (T2') do not suffer from reversibility effects, therefore the iron signal is not masked. Examples of improved phase contrast images for human MRI taken at 1.5T are shown in the Preliminary Section, Figures 7 & 8.

D.4.1.3. Procedures

An ongoing effort will be undertaken wherein we attempt to quantify MR imaged iron using known quantities of iron in different states in various inert configurations (phantoms). This information will be followed by imaging the IRP-2 knockout and control mice, which should represent all states of normal and aberrant iron accumulation. The imaged iron will be verified by absolute quantification of the various iron states obtained from microdissected mouse brain tissue using atomic absorption spectrometry. Tissue from additional mice in the study will be immunochemically labeled to obtain physical (morphometric and apoptotic) and quantitative information that parallels the endpoints used on human leukocytes described in aim 1 using laser scanning and confocal imaging. Specific endpoints are listed below, followed by the detailed methodology required to complete the endpoints.

D.4.1.4. Experimental Endpoints:

- MR Imaging/SWI.
- Analysis of iron containing phantoms using special sequences.
- Image analysis of IRP-2 deleted mice to identify "regions of interest" (ROI) with iron accumulation in brain.
- Quantitative histochemistry of iron in ROI in mouse brain tissue (heme iron, non-heme iron – NTBI, TBI, ferritin).
- Correlate iron measurements in specific ROI in mouse brain with MRI findings.
- Apoptosis as a function of age and iron accumulation in mouse brain tissue.
- Laser scanning cytometric quantification of ferritin, transferrin, transferrin receptor, β-amyloid, ubiquitin, and hemosiderin in mouse brain tissue.

D.4.1.5.1. Specific Methods

D.4.1.5.2. MR Imaging/SWI

Imaging will be done at 1.5T for humans and 4.7T for mice. Most susceptibility features are best imaged when the resolution is a factor of one to two times the size of the object. For this reason, in the human brain, we use the following parameters: TR = 67ms, susceptibility differences as small as 0.004 ppm can be measured with a 3D gradient echo method with a TE = 40ms and a resolution of 0.5 x 1.0 x 2.0 mm^3 (requiring a 5 minute scan time). Small structures like venules 300 to 500 microns are visible in the image because of their signal cancellation properties and their phase effects in the image. Small iron deposits in the basal ganglia are visible with this approach. These deposits are also less than 1 mm^3 in size but are still clearly visible. This exquisite sensitivity to micro-voxel effects is what makes SWI so powerful.

In addition to studying the distribution of iron in the brain, two additional MRI and MRS sequences to diagnose AD have been included to relate our MSI results to these two older MR techniques. The MRI sequence will be used to calculate hippocampal volume. The MRS sequence will be used to quantitatively observe a variety of metabolites in the hippocampus.

D.4.1.5.3. Imaging Protocol-Human

MR scans will be performed on a 1.5T VISION system (Siemens Medical Systems) with a UNIX based host computer (Sun Microsystems) with actively shielded gradients, and echo-planar capability. Prior to the scan the procedure will be explained in detail to each subject. Subjects will be positioned on the table with their canthomeatal line perpendicular to the table; head position stability is facilitated with

adjustable cushioned head supports. In addition to the three sequences used to study AD, axial FLAIR images will be obtained to diagnose neurological diseases which may mimic AD.

	TR/TE	ACQ	Matrix	Thick (mm)		Time (min)
MSI	57/40	1	512 x 512	2.0		9.5
MPRAGE	10/4	1	256 x 256	1.2		8.2
STEAM MRS	3000/20	1	NA	20x20x20		6.4
FLAIR	9000/119	1	256 x 256	5.0		5.0
					Total	29.1

Our experience is that older subjects up to at least 80 years of age, including those with mild MCI/AD, can tolerate durations of imaging up to 40 minutes without undue motion.

Axial and coronal images will be used for placement of spectroscopic single voxels (8 cc volume, 2x2x2 cm) located in the left and right hippocampal regions. Qualitative and quantitative H-1 MR spectroscopy will be performed with the product version of a stimulated echo acquisition mode (STEAM) sequence using a TR = 3000 msec, TE = 20 msec, 128 acquisitions, mixing time of 13.7 msec, 1024 data points, with CHESS water suppression. An additional eight acquisition spectrum without water suppression will be obtained and used for correction of eddy current-included phase shifts at each voxel location. Localized shimming and optimization of the water suppression pulses will be adjusted prior to acquiring each spectrum.

We are utilizing short echo time proton spectroscopy compared to long echo time MRS for several reasons. First, is the obvious advantage of obtaining signal from short T2 relaxation time metabolites such as myo-inositol and Glx, (glutamate + glutamine) as well as, NAA (n-acetylaspartate) are significantly decreased in both gray matter and white matter of patients with AD in post-mortem examination with MRS (85-87). Secondly, by using LCModel curve fitting software, we can overcome the problems associated with short TE spectra mentioned above to accurately fit the baseline and metabolite peaks for quantitation of metabolite levels. Lastly, short echo times minimize the signal decay due to both T2 and to coupling effects which benefits the quantitation process. No T1 and T2 corrections will be applied to the data because we feel that given the long TR and short TE used, the corrections would be very small and would not impact the results.

The raw T2 spin echo images will be transferred to Sun Workstations where the hippocampus will be manually segmented from adjacent structures. Following evaluation of the hippocampus the information will be transferred to a MS Word where data will be stored. The digital spectroscopy data will also be transferred to UNIX workstations for evaluation using the LC Model.

D.4.1.5.4. Imaging Protocol-Mouse

Imaging the mice will be performed on a Bruker Avance 4.7T imager with a head only volume coil. Using this higher powered field strength and smaller volume we expect to gain a factor of approximately 8 in SNR (over that obtained for humans) which we will use to reduce the voxel size to 0.5 mm x 0.5mm x 0.5mm by extending the time of data collection to 40 minutes we can reduce the voxel size to 0.25 mm x 0.25mm x 0.25mm. This will increase the resolution for differentiating structures within the mouse brain.

D.4.1.5.5. Analysis of Iron Containing Phantoms

Experiments will be performed on material with a known susceptibility to validate the ability of MRI to correctly quantify iron content within a given geometry. Three different shapes will be considered: first, a simple test tube will be imaged both parallel and perpendicular to the main field; second, a thin plane will be imaged; and third a thin plane warped to represent more the folds in the brain parenchyma will be imaged. These planes will be created using Mylar film to separate layers 2 to 3mm thick to mimic the human brain. The dimensions of these phantoms will be on the order of 10 cm on each side again to mimic the human brain and also to allow proper tuning and shimming of the phantoms. An agarose gel will be used as the filling material doped with several different iron carrying compounds with a series of different concentrations (first 100 nmol/gm and then 4 more times starting at 500 nmol/gm at increments of 500 nmol/gm up to 2000 nmol/gm) to mimic the iron in the brain. The susceptibility of each compound will be measured using the test tube shape since the effect of the geometry on phase under these conditions is well understood. Specifically, four different types of phantoms composed of a) FeCl-, b) FeSO4, c) ferritin, and d) hemosiderin will be prepared. These experiments will let us study the effect of concentration of iron for random systems (low concentrations are expected to have an exponential effect on signal loss while high concentrations are expected to be more geometry dependent). The brain's structure and iron concentration does not appear to have the usual geometry effect as the sulci phase is found to be rather uniform, independent of the folding that occurs. This may indicate a low concentration and, hence, an easy means to calibrate the phase independent of object shape. These experiments will be carried out at both 1.5T and 4.7T to ensure that the linear behavior is present and that there are no special calibrations required from one field strength to the next.

D.4.2.1.1. Animal Model

Transgenic mice will be shipped from Dr. Rouault's laboratory at NIH (Bethesda, MD) and maintained at the Loma Linda University Medical Center's Animal Care Facility under an approved protocol. These mice display neurodegenerative symptoms progressively within their first 6 months of age. The mice typically manifest ataxia, vestibular dysfunction tremors and postural abnormalities among others detectable neurological changes which progressively increase with brain iron up to 18 months of age. Mice will be on a twelve-hour light-dark schedule with food and water *ad Librium*. The mice will be observed for skin irritation, oral mucosal, behavioral, and neurologic signs of stress. All animals will be weighed weekly, once changes are noted the inspections frequency will be increased according to the severity of the symptoms. At selected intervals, animals will be anesthetized for neuro-imaging using isoflurane inhalation (4% induction, 1% maintenance) and placed into an MRI compatible stereotactic apparatus. Rectal temperature will be monitored continuously and maintained at 37 ± 0.5 °C with a warm water coil placed underneath the animal.

To optimize the MRI sequences above, we will image mice from 4 groups: a) controls (C57bl/6), b) Ireb2+/+, c) Ireb2+/-, and d) Ireb2-/- mice, 6 mice per group will be processed over an 18 month period. Sampling will take place at 1, 3, 6, 9, 12 and 18 months to understand the spatial and temporal deposition of iron within the brain. Post MR imaging 3 mice from each group will be processed for quantifying brain iron and 3 from each group will be processed for immunocytochemical quantification for apoptosis and iron-regulated proteins Section D.4.2.1.5.

D.4.2.1.2. MRI Analysis

Image analysis is performed for each mouse on a single slice immediately anterior to the slice where the hippocampus can be seen curling inferiorly. This position corresponds approximately to the bregma -3.60 mm and maximized the cross-sectional area of each region of interest (ROI). Cheshire™ image

processing software (Hayden Image Processing Group, Waltham, MA) will be used to outline and analyze the ROI's that are confirmed by a second researcher. The bilateral ROI's included the amygdala (and associated nuclei), piriform cortex (including part of the entorhinal and perirhinal cortices), hippocampus, retrosplenial cortex (including motor and somatosensory cortices) and thalamus. A two pixel width separated the hippocampi and retrosplenial ROI's. A line drawn across the bottom of both hippocampi that extended across the cortex demarcated the inferior border of the retrosplenial ROI. The piriform and amygdala ROI's abutted each other and extended the same distance superiorly and inferiorly. Medially two to four pixels separated the thalamus from the amygdaloid ROI, to minimize signal contribution from the lateral ventricle. A 5 by 5 pixel square will be centered within the thalamus. For the 3D gradient echo images, information from slices around this slice will also be evaluated.

T2 values from the magnetic susceptibility images will be obtained from the precentral gyrus, deep nuclei including the putamen and globus pallidus, thalamus, and hippocampus, which will correspond to areas being analyzed in the animal model. T2 values will be obtained over an area of 50 voxels from regions in these structures and recorded. Subjective evaluations will also be done in these structures to estimate the distribution of iron.

The hippocampus will be semiautomatically segmented to obtain their volumes. Our group has done this in both adults and children (88, 89) using Chesline™ to define regions of interest. We will normalize these results to intracranial volumes to minimize variation due to age and sex.

A frequency-domain curve fitting method, LCModel, will be used for analysis of spectra. This software is presently installed and runs on the Sun Microsystems platform available on a satellite console with our commercial scanner. Fourier transformation of data will be performed without zero-filling or apodization followed by approximate zero-order phasing in order to provide a good starting point for LCModel analysis software. The output of the analysis will provide quantitative values for cerebral metabolites of interest for the study which include N-acetylaspartate (NAA at 2.02 ppm) glutamine (Glx between 2.1-2.5 ppm), creatine and phosphocreatine (Cre at 3.0 ppm), choline and choline containing compounds (Cho at 3.2 ppm), myo-inositol (mIo at 3.56 ppm), as well as, metabolite ratios. In LCModel analysis, quantitation is achieved by fitting spectra as a linear combination of model spectra acquired with a very high signal-to-noise ration (SNR) and a narrow linewidth using similar hardware and software. This "basis set" of spectra is provided with LCModel software. To calibrate metabolite concentrations for local machine performance and to monitor possible fluctuations, we will use a 300 cc spherical phantom containing known metabolite concentrations of NAA, Cre, Cho and myo-inositol on a weekly basis under controlled conditions. Advantages of LCModel is its ability to deal with the baseline contributions from macromolecules, moderate lips contamination and variable water suppression often encountered in short TE spectra.

D.4.2.1.3. Statistical Analysis of the MR Data

Left and right comparison of the bilateral ROI's will be performed for each animal using a one-way ANOVA ($p < 0.05$). A two-tailed student's t-test (significant at $p < 0.05$, highly significant at $p < 0.01$) will then be performed to compare the control values with the experimental values at each time point.

D.4.2.1.4. Extracting Absolute Iron Content from MRI

Specifically, we will run a multi-echo, gradient/spin echo combination defined as follows. First create a spin echo structure with a TE of 80ms. About this echo time, collect a series of 31 echoes of the same polarity (an echo every 2.5ms). We have both theoretically predicted, and experimentally verified, the

following theory. The signal behavior for a random set of spheres (which is an excellent approximation for iron (which is known to conglomerate in spherical shapes) especially given the large voxels we are using) is given by:

$S(t) = \rho(1-\lambda)\exp(-0.4l(t\,\delta\omega)^2)$ for $t\,\delta\omega < 1.5$
and
$S(t) = \rho(1-\lambda)\exp(-it\Delta\omega)\exp(-R2'\text{abs}(t-t_s))$ for $t\,\delta\omega > 1.5$
where
$\delta\omega = \gamma 4\pi(M-M_o)/3$, $R2' = 1.21\,\lambda\,\delta\omega$, $t_s = 1/(1.21\,\delta\omega)$ and $\Delta\omega = -0.16\,\lambda\,\delta\omega$.

By measuring the short time and long time components, we can get a numerical estimate for the arguments in each exponential and, therefore, for $(M-M_o)$ (extracted from dw) and for λ (extracted from R2' since $\delta\omega$ is now known). For example, for magnetic particulates used as contrast agents in MRI, such as AMI 225, $\delta\omega$ has the value 3.4×10^{-7} /s. Using a volume fraction of $\lambda = 2 \times 10^{-6}$ yields an R2' of 82.23/s in excellent agreement with other estimates (which range from 80 to 100/s from numerical simulations). Note that when the susceptibility is known, R2' can be used directly as a measure of the volume fraction λ. Now for much smaller susceptibilities on the order of ppm, such as diamagnetic or paramagnetic substances, then $\delta\omega$ is on the order of ms. For example, for a vein with haematocrit of 0.4 and oxygen saturation of 55%, the value of $\delta\omega$ is about 3 ms. Ironically, the smaller the susceptibility, the longer $\delta\omega$ and when t_s lies between 3 and 30 ms after or before the spin echo, the signal can now be used to find the susceptibility of the source producing the signal loss as well as its volume content. Since we plan to measure the susceptibilities of each of the components found to be responsible for the signal loss (ferritin, etc.) we do not need this feature. However, there is another numerical estimate we can make and that is for the phase term $-0.16\,\lambda\,\delta\omega$ which is directly related to R2' and so it adds no new information when there is only one source of magnetic field variation. However, if non-heme iron is not the only source and heme iron contributes through the vein mechanism referred to above, then these two may no longer be related and we will see the temporal response measured about the echo as looking like a parabola. From this we can then use a two-parameter model in an attempt to extract the heme from non-heme iron. Finally, as a means to accomplish this unambiguously, we will use a contrast agent to modify the local susceptibility in a known way and repeat the experiment.

The above results will also be compared with T1, T2 and diffusion weighted imaging to touch base with previous measurements in the field. The multi-echo, spin echo sequence described in the animal model section will be used to measure T1. A 3D variable angle method and a conventional 2D multiple IR sequence will be used to estimate T1 values.

A complete error analysis will be performed for each of the four measurements phase, R2', R2 and R1. We will look for any discrepancies between the methods in both normal individuals and experimental subjects. As described earlier, signal recovery can occur in a number of instances which ruin the correlation with iron for R1 and R2 methods while our theory suggest that this will not be the case for phase or R2'.

D.4.2.1.5. Quantitative Histochemistry of Iron in ROI in Mouse Brain Tissue (heme iron, non-heme iron – NTBI, TBI, ferritin)

MRI analysis will be performed 6 times during an 18-month period. Once the MRI series is complete a subset of three mice will be euthanized by the technique of Lowry (90). Blood and brain tissue will be removed from selected mice after decapitation. The decapitation technique of Lowry enables the snap freezing of brain with preservation of labile metabolites for further analysis after tissue lyophilization. Three mouse heads from each group will be placed immediately after resection into Freon-12 (CCl_3F_2)

chilled to near its freezing point (-156°C) by liquid nitrogen and stored at -50°C until sectioned and dissected in a cryostat at -20°C. The brains are dissected free and sectioned at 20 μ in a cryostat at -20°C. Axial cuts of brain from designated regions corresponding to MRI cuts are dried in a 5 μ Hg vacuum at -30°C for 12 hours. Controlled regional dissection of selected areas and regions of interest is performed at room temperatures at 80X magnification employing micromanipulating tools and methods of Lowry (91). Dissected samples and sections are stored under vacuum at -50° C until assayed.

Dissected samples from the regions of interest will be approximately 200 x 200 x 30 microns and weigh approximately 2-3 μg. The highest content of brain iron in the normal human brain is in the globus pallidus – 20-21 mg/100 gm in the globus pallidus with the partition between high molecular weight (ferritin), intermediate (transferrin), and low molecular weight (non-tranferrin bound iron NTBI) variable and uncertain in view of rapid mobilization with oxidative stress. Based on previously measured values in normal brain, anticipated amounts of total brain in 3 μg specimens of lyophilized mouse brain are 0.2 to 0.3 μg. After weighing of the lyophilized samples on a calibrated quartz microfiber balance, samples will be transferred to the bottom of reaction tubes (4.0 cm length, 1.5-2.5 mm I.D.) using precautions to prevent iron contamination.

The method of Jakemam *et al.* (92) will be used to measure non-transferrin-bound iron (NTBI), transferrin, ferritin bound iron as well as total iron in the 3γ sample. This technique of atomic absorption spectrometry has a functional detection limit of 0.1 μmol/L for 25 μl injection volume and is capable of detecting 2.5 x 10^{-6} μmoles of Fe, well within our expected range of values in the 3 μg lyophilized mouse brain, 1 x 10^{-3} μmoles of iron total with partitions uncertain. Our assays with the Caltech plasma atomic absorption spectrometer on the extracted lyophilized brain will enable determination of steady state levels of total iron, NTBI, TBI, and ferritin.

D.4.2.1.6. Apoptosis as a Function of Age and Iron Accumulation in Mouse Brain Tissue and Laser Scanning Cytometric Quantification of Ferritin, Transferrin, Transferrin Receptor, β-Amyloid, Ubiquitin, and Hemosiderin in Mouse Brain Tissue

The animals will be euthanized and bled with the blood pooled per group and processed to isolate leukocytes, similar to that previously described for human blood. A serum sample from the mice will also be archived frozen -70^0c for future experiments. The brains will be separated into right and left hemispheres, weights recorded (wet weight) and, randomly, one hemi-brain from each animal will be placed in plp (4% buffered formalin solution) and the other half placed in cryoprotectant and frozen (protected from desiccation). The frozen brain tissue will be sectioned and every third section from the front (level 1), middle (level 2) and the back (level 3) will be placed on poly-l-lysine coated slides. The figure below shows the structures present in each of the three levels.

Level 1-Front-section

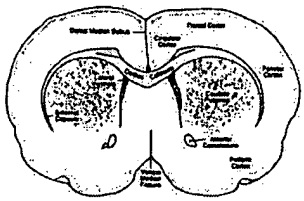

Schematic shows cerebral cortex, lateral ventricles, corpus callosum and caudate putamen

Level 2-Mid-section

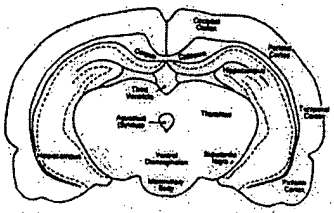

Schematic shows cerebral cortex, thalamus, third ventricle and hippocampus

Level 3-Back-section

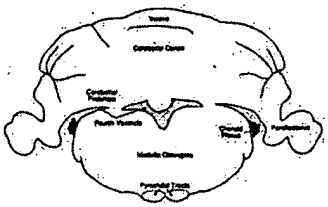

Schematic shows cerebellum, medulla, fourth ventricle and pyramidal tracts

5-10 μm sections will be made from each hemi-brain (in triplicate: 1 set for H&E, 1 set for apoptosis, and 7 sets for immunocytochemistry using; anti-IRP-1, anti-IRP-2, anti-ferritin, anti-transferrin receptor, β-amyloid ubiquitin and hemosiderin.

D.4.2.1.7. H&E and Apoptosis Measurements

One 5-10 μm-tissue section from each of the three brain levels will be stained with H&E for morphologic assessment of the tissue (74). One set of each brain tissue sections will be labeled using an Apodirect assay modified as described by Green *et al.* (73). DNA damage will be used to assess late apoptotic events in the brain tissue using terminal deoxynucleotidyl-transferase (TdT) mediated fluorescent (FITC)-conjugated BrdU incorporation into free 3' ends of nucleic acids. Briefly, tissue will be fixed in -20^{0}C 70% ethanol for 15 minutes. The fixed tissue will be re-hydrated in PBS for five minutes and incubated with a mixture of TdT, reaction buffer and FITC-BrdU provided with the kit. Tissue will be incubated with the DNA labeling mixture overnight at room temperature (22-24^{0}C), washed and counter-stained for 30 minutes with propidium iodide (PI)/RNAse, washed and protected with permafluor and covered with glass coverslips. FITC-BrdU incorporation will be quantified using a laser scanning cytometer (LSC) (CompuCyte, Cambridge, MA) as described below.

D.4.2.1.8. Immunocytochemical Labeling of Frozen Tissue Sections

Tissue will be fixed as described above for the apoptosis assay. The fixed tissue will be labeled with primary antibodies (anti-IRP-1, anti-IRP-2, anti-ferritin, anti-transferrin/transferin receptor, β-amyloid ubiquitin and hemosiderin). Incubation with primary antibodies/antisera will be 16 hrs at 4^{0}C, followed by washing in PBS containing 0.05% Tween-20 (PBST). Antibodies that are not directly conjugated to a fluorescent molecule will be secondarily labeled with alexa-488, alexa-594, Cy-2 or Cy-5 anti-mouse or rabbit IgG antibodies for a minimum incubation period of 4 hrs at 25^{0}C. Just prior to completion of the secondary antibody incubation, DAPI (1 μg/ml) or propidium iodide (PI, 5 μg/ml), depending on the ability to dual label and/or confocal microscopy as the analytical endpoint, will be added for 10 min. Excess secondary antibody and nuclear counterstain will be removed by washing in PBST and the tissue protected with permafluor and glass coverslips, allowed to dry flat in the dark prior to quantitative analysis (LSC and Confocal microscopy as described below) and photography. Non-specific fluorescence will be determined by incubating control sections with non-immune sera and secondary antibody, or secondary antibody alone.

D.4.2.1.9. Laser Scanning Cytometric (LSC) Quantification of Immuno-fluorescence/ Confocal Microscopy for Intracellular Localization

The LSC has an Olympus BX50 base and is configured with argon ion, helium-neon and UV lasers for 6-color analysis. There are four sensors, simultaneously digitized at 625,000 Hz corresponding nominally to 0.5-micrometer spatial intervals along the scan. Fluorescent energy is collected by the

objective, reflected by a partially silvered mirror to allow the CCD camera to image the cells and steered through a scan lens to the scanning mirror. 4 photo-multiplier tubes, each capable of detecting a specific range of fluorescent wavelengths, support dichroic mirrors and optical interference filters. The fluorescent measurements and x, y coordinates are recorded digitally and stored as FCS files in the computer base. An example of an X, Y map of fluorescent-labeled brain tissue is shown in the preliminary data section Figure 10. Tissue to be analyzed is contoured by the labeled nucleus. A variety of gating parameters can be chosen, but will include those that collect information on signal intensity versus cell size, cell number (area, perimeter, count, etc). Protocol settings and display parameters will be optimized using control positive and negative samples, the optimized protocol and display files will be stored and utilized in scanning replicate sections.

The quantity of specific proteins is an important parameter that will be measured by the LSC. However, many proteins have discrete locations that coincide with their functional properties, thus, a better understanding will be gained by the cellular/subcellular localization of specific proteins. Localization will be achieved with confocal microscopy. Fluorescently labeled tissue sections will be imaged in 3-dimension using an Olympus IX-70 based, BioRad-1024 confocal microscope. Sections will be acquired with low power (4-20x) in 0.5mm z-steps for general distribution, and high power (40-100x) magnification for acquiring cellular/subcellular location of the proteins listed above.

D.4.2.1.10. Expected Results/Alternatives MRI Component of Research

In terms of iron content extraction from the MRI data we expect to see a linear increase in T2' measurements as iron concentration increases, especially given all the work that has been done in the last decade showing that even the T2 effects are linear with field strength. We have the theoretical understanding and methodology to accomplish this via an extraction of T2' from T2 and T2* data. Further, our own preliminary data on the spleen shows that the tissue has a high spin density, a long T1 and a long T2 (similar to what happens in restoration of substantia nigra signal) and yet it has a very short T2'. This may be caused by the heavy blood product deposition that takes place in the spleen. Given the ambiguities present in the signal restoration discussed earlier, these results bode well for the success of our approach in measuring iron content.

D.4.3. Error Analysis of Phase in Phantoms, Animals and Humans

Current iron concentration differences between gray matter and white matter are manifest as roughly 20 degrees in 40 ms, which corresponds to roughly 0.1 ppm. If the SNR in the magnitude image is only 15:1 then the standard deviation of the phase is 0.06 radians (4° or 0.002 ppm) or roughly a 10% error. One could then imagine evaluating susceptibility differences greater than 3 standard deviations, which corresponds to 0.006 ppm with a p value of 0.005. This depends very much on the experiment run and could in theory be further improved by averaging the data. This averaging can be accomplished in two ways. First, more data could be acquired or if there are multiple pixels exhibiting the same behavior the data could be filtered. Practically, the answer to this will depend on the resolution required. For if a lower resolution is sufficient, then the SNR can be dramatically improved per unit time by running the experiment with lower resolution to enhance the SNR. For example, an MR scans with the resolution of 0.5 x 1.0 x 2.0 $mm^3$and a TE = 40ms takes 5 minutes to acquire and yields the values quoted above. However, if a resolution of 1 x 2 x 2 mm^3 is sufficient, then the scan takes half the time and yields 2 times higher SNR. So if the same 5 minutes were used, the increase in SNR is 2sqrt(2) tantamount to imaging at field strength 8 times higher. We will examine resolutions varying from 0.25 microns to 1 mm in the phantoms and animals to determine the most efficient and yet most appropriate set of imaging parameters.

A similar argument holds for human studies. We propose using several sets of imaging parameters on the first 10 subjects. These will include echo times of 40, 80 and 120 ms in order to evaluate the *in vivo* sensitivities. We will then vary the resolution from 0.5 x 0.5 x 1.0 mm^3 to 1 x 1 x 2 mm^3 in order to study the sensitivity as a function of voxel size. On the higher resolution images, we will filter the data back to a lower resolution image by a factor of two in each direction to compare with the lower resolution data. There are a number of reasons for this, as the MR process is non-linear in a number of ways. First, Gibbs ringing is reduced relative to the lower resolution scan. Second, the effects of field inhomogenities are reduced. And, third, scale invariance effects can be checked (what may be visible at the high resolution may not be at the lower resolution). Volunteer studies will be performed in the first year on five healthy volunteers and five recruited patients. This allows us to use some of the patient results independent of which echo times and resolution are finally decided upon later.

D.4.4.1. Potential Difficulties: Improvement of Background Phase Elimination

Another simple approach to remove all linear phase effects is to use a double echo method. Here the phase from the first echo is used to predict the phase from the second echo based upon the simple linear dependence of phase expected from background phase effects. If the phase of the first echo, $\gamma\Delta BTE1$, is multiplied by TE2/TE1 to predict $\gamma\Delta BTE2$, and the predicted phase subtracted from that of the second echo (usually accomplished by complex division) then the expected phase of the corrected image will be zero. This then will leave behind any non-linear effects associated with a two-compartment model where the phase effects are not simply additive. This makes it possible to separate small local within pixel effects.

D.4.4.2. Potential Difficulties: Separating Non-heme from Heme Iron in Animals and Humans

We will use our theory to estimate the phase expected from heme and non-heme sources using the known estimates for the susceptibility of ferritin and its concentration of 1450nmol/gm taken from the red nucleus. To accomplish this, we will use a multi-echo spatial technique to quantify the heme component. The heme iron will reveal itself as an oscillatory effect for blood but not for free iron or iron in ferritin. This technique is sensitive to partial volume effects coming from venous blood and should be distinct from the effects caused by a uniform distribution of iron in the brain parenchyma. We will also perform the same sequence with a blood nulling technique in which case if the oscillatory effects vanish we will have ascertained that they were caused by blood in the first place. This will allow us to quantify how much of the phase behavior comes from heme iron (if any) versus free iron or iron bound in ferritin. We can also validate the effects of blood by putting in a known quantity of contrast agent (the conventional agents have a phase effect of 1°/mM/ms) to mimic the susceptibility of blood. By doubling the effect of blood we can get an estimate as to what the effect of blood itself is on the phase. Finally, there is an issue of resolution and scale dependence. If some phase effects come from major vessels they will manifest themselves differently for different resolutions. We will run the experiments at resolutions ranging from 0.5 to 2mm in humans and 0.25 to 1mm in animals to determine if there is any effect of voxel size on the measurements. Any changes to the phase of the image in the parenchyma or in the critical time t_s will be a marker of the blood's contribution. These sequences will be performed on animals and humans using a different set of 5 normal volunteers to those referred to above.

D.4.4.3. Potential Difficulties: Calculating Baseline Susceptibilities

A careful study of the phase behavior and the ability of the phase filter to remove background material will be made. Since the filter used is a high pass filter there will be a loss of DC information. As this is important to the quantification of the susceptibility (differences between tissues is not highly affected), the ability to extract the DC level phase will also be examined and compared with the original unfiltered

data. To ensure an absolute measure of phase, not just phase differences, reference markers of known susceptibility will be imaged with the animals and humans if necessary.

D.5.1. Specific Aim #3. Combine the Data Obtained in the Aims 1 and 2 with Periodic Psychometric Evaluations of the Subject Populations (MCI) at Risk for AD to Determine Relationships and/or Correlations Between Serial *ex vivo* Blood Markers, MR Brain Iron Quantitation, and Clinical Course

D.5.2. Key Hypothesis: Altered brain iron metabolism in the face of aging and MCI is a significant risk factor for AD, and this process can be analyzed by new, minimally invasive technologies that evaluate steady state brain iron metabolism.

D.5.3. Location of Work: Loma Linda University and BioErgonomics Inc.

D.5.4. Key Endpoints:

- Clinical course of dementia as monitored by sequential psychometric tests
- Correlation of MRI of brain iron determined sequentially
- Correlation of peripheral blood biological markers with clinical course
- Autopsy

Blood samples will be drawn in Dr. Larsen's clinic after enrollment of the subject into the BRP research program. Blood samples will be drawn twice yearly when an accelerated deteriorating clinical course is manifested. Psychometric exams will be done once per year unless clinical deterioration is noted and then repeated at a rate consistent with the clinical course. The longitudinal follow-up psychometric examinations will also include functional impairment of activities of daily living (ADL's). Though basic ADL's are not impaired until dementias advance, more complex and demanding activities such as money management, appliance use, and household chore performance tend to be impaired at a much earlier basis. The specific psychometric tests are discussed in Section D.2.3. and are standard and conventional evaluations for monitoring a dementing illness.

MCI subjects will be followed with no restrictions on their therapy or nutritional supplements. A rapport will be established with the subject and family members in order to gain access to age-matched "normal" controls to enroll in the study. In the event of death, an effort will be made to obtain an autopsy and permission to examine the brain. Dr. Norman Peckham, a board certified neuropathologist, will conduct the brain post- mortem examination according to guidelines established by CERAD (80).

As noted above, clinical members of the BRP will meet once per week for a 2 hour period to discuss and evaluate data for each subject to include flow cytometric tests.

D.5.5. Correlation of Flow Cytometric Data and Patient's Clinical Status

The flow cytometric data will be correlated with the clinical status of the patient in a separate filing system with a data sheet for each patient. Correlation of relative expression of IRP-2 and severity of disease will be analyzed by regression analysis. Expression of IRP-2, expression of transferrin receptors, spontaneous and stimulated apoptosis will be assessed in conjunction with severity of disease by analysis of variance (ANOVA). Spontaneous and stimulated pro-inflammatory cytokine expression will be compared between the patient and cohort group by Student's t-test. The correlation of severity of disease with the existence of IRP-2 polymorphisms will be analyzed by ANOVA.

D.6. Sample Size and Statistical Analysis

The major outcome of this study is the correlation of :
a. Psychometric scores (the "gold standard")
b. Results obtained from blood (BAP, IRP-2, inflammatory cytokines, and apoptosis)
c. Quantification of iron in the brain obtained from MRI

with the ultimate twin goals of: (1) much earlier detection of subjects at risk than is now possible using psychometric testing, and (2) revealing basic biochemical relationships which may exist between the three outcomes mentioned above.

Outcome data will be collected on the subjects at fixed times over 3-4 years and will be analyzed in two phases: (a) correlations at intermediate time points during the study, and (b) as a repeated measures model and a logistic regression model at the conclusion of the study.

Ultimately, 100 subjects will be followed: 75 which have a beginning diagnosis of MCI. Of these, approximately 50% (30-40) are expected to convert to AD. Of the twenty-five controls, we expect approximately 5% (1-2) to convert. At the end of the study we should have at least 35 subjects which have converted.

Bi-variate and multiple correlation models will be used to detect possible associations between psychometric scores and the other outcomes. A sample size of 100 will allow us to determine a $R^2 = 0.1$ significant with 85% power (assuming a standard error of 0.1) which is far more than adequate for our research.

At the end of the study, all subjects will, using the gold standard, be classified as demented/not demented. Two group Repeated Measures ANOVA will be used to investigate time effects which may be significant in the outcome measures. A logistic regression model will be used to investigate the odds of disease associated with each of the predictor variables (or changes in the predictor variables, b and c above). In addition to the logistic model it may be possible to use a Cox regression model (survival analysis) with "time to confirming diagnosis" as the dependent variable. This will increase our power by being able to include subjects which are lost to follow-up.

Much of this project involves basic research on variables where the clinically significant effect size is not known, and in some cases even a measure of variation is not known (e.g. MRI data), therefore the appropriate sample size for some of the analysis is difficult to determine. However when compared to other studies of this type, our sample size of 100 is large. Probably most important, our study will yield variation estimates in variables which have never been studied or measured as we propose to do. This will be important information for use in sample size determinations on future studies.

E. Human Subjects

We have approval from the Loma Linda University Institutional Review Board for the study of our cognitively impaired patients. The approval number is 40133. The protocol is currently being amended to include all the MRI and psychometric tests described in this proposal. These procedures entail little or no risk to the patient. All data will be coded and kept confidential. Each subject will sign an informed consent.

F. Vertebrate Animals

This project involves *in vivo* experiments in which mice are subjected to MR imaging over a three-year period. 300 transgenic mice will be studied by a procedure with minimal pain. We anticipate studying 100 mice per year in order to attain the statistical significance necessary to document and validate tissue iron concentrations with MR images. Approval for this study from our institutional animal research committee is pending. Use of *in vivo* studies is necessary because it is the only feasible way to determine steady-state brain iron levels in order to make correlation with human MR images.

Overseeing the animals' care at LLU before MR imaging will be the responsibility of Charles Kean, DVM and the team of investigators. Mice will be decapitated immediately after the MRI while still under anesthesia in order to snap freeze the brains for quantitative histochemical determinations. This procedure is consistent with recommended practices of the American Veterinary Association Council on Euthanasia and involves minimal distress to the animals.

G. Literature Cited

1. The Ronald and Nancy Reagan Research Institute of the Alzheimer's Association and the National Institute on Aging Working Group. Consensus report of the working group on: "Molecular and Biochemical Markers of Alzheimer's Disease." Neurobiology of Aging 1998; 19(2): 109-116.
2. Kennard, M.L., Feldman, H., Yamada, T. and Jeffries, W.A. Serum levels of the iron binding protein p97 are elevated in Alzheimer's disease. Nat Med. 1996; 2(11): 1230-1235.
3. Serrano Sanchez, T., Robinson Agramonte, M., Lorigados Pedre, L., Diaz Armesto, I., Gonzalez Fraguela, M.E. and Dorta-Contreras, A.J. Endogenous nerve growth factor in patients with Alzheimer's disease. Rev Neuro. 2001; 32(9): 825-828
4. Arai, H. Nakagawa, T., Kosaka, Y., Higuchi, M., Matsui, T., Okamura, M. and Sasaki, H. Elevated Cerebrospinal fluid Tau protein level as a predictor of dementia in memory impaired individuals. Alzheimer's Research. 1997; 3:211-213.
5. Trojanowski, J.Q., Clark, C.M., Arai, H. and Lee, V. Elevated levels of tau in cerebrospinal fluid: implications for the ante mortem diagnosis of Alzheimer's disease. Alzheimer's Disease Review. 1996, 1:77-83
6. Jung, S.S., Gauthier, S. and Cashman, N.R. Beta-amyloid precursor protein is detectable on monocytes and is increased in Alzheimer's disease. Neurobiology of Aging. 1999; 20:249 257.
7. Cao, X. and Sudhof, T.C. A transcriptively active complex of APP with Fe65 and histone acetyltransferase Tip60. Science. 2001; 293(5527): 115-120.
8. Matiba, B., Mariani, S.M., and Krammer, P.H. The CD95 system and the death of a lymphocyte. Semin Immunol. 1997; 9:59-68.
9. Schindowski, K., Leutner, S., Muller, W.E. and Eckert, A. Age-related changes of apoptotic cell death in human lymphocytes. Neurobiology of Aging. 2000; 21:661-670
10. Phelouzat, M.A., Laforge, T., Arbogast, A., Quadri, R.A., Boutet, S. and Proust, J.J. Susceptibility to apoptosis of T-lymphocytes from elderly humans is associated with increased *in vivo* expression of functional Fas receptors. Mech Ageing Dev. 1997; 96:35-46
11. Butterfield, D.A., Howard, B., Yatin, S., Koppal, T., Drake, J., Hensley, K., Aksenov, M., Aksenova, M., Subramaniam, R., Varadarajan, S., Harris-White, M.E., Pedigo, N.W. and Carney, J.M. Elevated oxidative stress in models of normal brain aging and Alzheimer's disease. Life Sci. 1999; 65(18-19): 1883-1892.
12. Griffiths, P.D. and Crossman, A.R. Distribution of iron in the basal ganglia and neocortex in postmortem tissue in Parkinson's disease and Alzheimer's disease. Dementia. 1993; 4(2): 61-65.
13. Loeffler, D.A., Connor, J.R., Juneau, P.L., Snyder, B.S., Kanaley, L., DeMaggio, A.J., Nguyen, H., Brickman, C.M. and LeWitt, P.A. Transferrin and iron in normal Alzheimer's disease, and Parkinson's disease brain regions. J Neurochem. 1995; 65:710-716.
14. Smith, M.A., Wehr, K., Harris, P.L.R., Siedlack, S.L., Connor, J.R. and Perry, G. Abnormal localization of iron regulatory protein in Alzheimer's disease. Brain Research. 1998; 788:232-236.
15. Good, P.F., Perl, D.P., Bierer, L.M. and Schmeidler, J. Selective accumulation of aluminum and iron in the neurofibrillary tangles of Alzheimer's disease: a laser Microprobe (LAMMA) study. Ann Neurol. 1992; 31:286-292.
16. Behl, C. Alzheimer's disease and oxidative stress: implications for novel therapeutic approaches. Prog Neurobiol. 1999; 57(3): 301-323.
17. Yanker, BA. Mechanisms of neuronal degradation in Alzheimer's disease. Neuron. 1996; 16:921-932.

18. Rottkamp, C.A., Raina, A.K., Zhu, X., Gaier, E., Bush, A.I., Atwood, C.S., Chevion, M., Perry, G. and Smith, M.A. Redox-active iron mediates amyloid-beta toxicity. Free Radic Biol Med. 2001; 30(4): 447-450.
19. Sayre, L.M., Perry, G., Harris, P.L.R., Liu, Y., Schubert, K.A. and Smith, M.A. In situ oxidative catalysis by neurofibrillary tangles and senile plaques in Alzheimer's disease: a central role for bound transition metals. J Neurochem. 2000; 74(1): 270-279.
20. Roses, A.D. Causes or consequences of inflammation and pathological signs of Alzheimer's disease. Neurobiol Aging. 2000;21(3):423-425.
21. Shoham, S. and Youdim, M.B. Iron involvement in neural damage and microgliosis in models of neurodegenerative diseases. Cell Mol Biol. 2000; 46(4): 743-760.
22. Bayer A.L., Baliga, P., Woodward, J.E. Transferrin receptor in T cell activation and transplantation. J Leukocyte Biol. 1998; 64(1): 19-24
23. Smith, M.A., Harris, P.L.R., Sayre, L.M. and Perry, G. Iron accumulation in Alzheimer disease is a source of redox-generated free radicals. . Proc Natl. Acad Sci USA. 1997; 94:9866-9868.
24. Connor, J.R. and Benkovic, S.A. Iron regulation in the brain: histochemical, biochemical, and molecular considerations. Ann Neurol. 1992; 32Suppl:S51-S61.
25. Benkovic, S.A. and Connor, J.R. Ferritin, transferrin, and iron in selected regions of the adult and aged rat brain. J Comp Neurol. 1993; 338(1): 97-113.
26. Cairo, G., Taccini, L., Pogliaghi, G., Anzon, E., Tomasi, A. and Bernelli-Zazzera, A. Induction of ferritin synthesis by oxidative stress. Transcriptional and post-transcriptional regulation by expansion of the "free" iron pool. The American Society for Biochemistry and Molecular Biology. 1995; 270(2): 700-703.
27. Beard, J.L., Connor, J.D. and Jones, B.C. Brain iron: location and function. Progress in Food and Nutrition Science. 1993; 17:183-221.
28. St≅ubli, A. and Boelsterli, U.A. The labile iron pool in hepatocytes: prooxidant-induced increase in free iron precedes oxidative cell injury. AJP – Gastrointest and Liver Physiol. 1998;274(6):G1031-G1037.
29. Rouault, T.A., Hentze, M.W., Caughman, S.W., Harford, J.B. and Klausner R.D. Binding of a cytosolic protein to the iron-responsive element of human ferritin messenger RNA. Science. 1988; 241:1207-1210.
30. Iwai, K., Drake, S.K., Wehr, N.B., Weissman, A.M., LaVaunte, T., Minato, N., Klausner, R.D., Levine, R.L. and Rouault, T.A. Iron-dependent oxidation, ubiquitination, and degradation or iron regulatory protein 2: implications for degradation of oxidized proteins. . Proc Natl. Acad Sci USA. 1998; 95(9): 4924-4928.
31. Smith, M.A., Wehr, K., Harris, P.L.R., Siedlack, S.L., Connor, J.R. and Perry, G. Abnormal localization of iron regulatory protein in Alzheimer's disease. Brain Research. 1998;788:232-236.
32. Pinero, D.J., Hu, J. and Connor, J.R. Alterations in the interaction between iron regulatory proteins and their iron responsive element in normal and Alzheimer's diseased brains. Cell Mol Biol. 2000;46(4):761-776.
33. Lesnikov, V., Lesnikova, M. and Deeg, H.J. Pro-apoptotic and anti-apoptotic effects of transferrin and transferrin-derived glycans on hematopoietic cells and lymphocytes. Exp Hematol. 2001;29(4):477-489.
34. Combs, C.K., Karlo, J.C., Kao, S.C., and Landreth, G.E. Beta-amyloid stimulation of microglia and monocytes results in TNF alpha-dependent expression of inducible nitric oxide synthase and neuro apoptosis. J Neurosci. 2001;21(4):1179-1188.
35. Bianca, V.D., Dusi, S., Bianchini, E., Dal Pra, I. and Rossi, F. Beta-amyloid activates the O-2 forming NADPH oxidase in microglia, monocytes, and neutrophils. A possible inflammatory mechanism of neuronal damage in Alzheimer's disease. J Biol Chem. 1999;274(22:15493-15499.

36. Iwai, K., Klausner, R.D. and Rouault, T.A. Requirements for iron-regulated degradation of the RNA binding protein, iron regulatory protein 2. EMBO J. 1995;14(21):5350-5357.
37. Hoozemans, J.J., Rosemuller, A.J., Veerhuis, R, Eikeleboom, P. Immunological aspects of Alzheimer's disease: therapeutic implications. BioDrugs. 2001;15(5):325-337.
38. Lue, L.F., Rydel, R., Brigham, E.F., Yang, L.B., Hampel, H., Murphy, G.M. Jr., Brachova, L., Yan, S.D., Walker, D.G., Shen, Y. and Rogers, J. Inflammatory repertoire of Alzheimer's disease and nondemented elderly microglia *in vitro*. Glia. 2001;35(1):72-79.
39. Shaw, K.T., Utsuki, T., Rogers, J., Yu, Q.S., Sambamurti, K., Brossi, A., Ge, Y.W., Lahiri, D.K. and Greig, N.H. Phenserine regulates translation of beta-amyloid precursor protein mRNA by putative interleukin-1 responsive element, a target for drug development. Proc Natl Acad Sci USA. 2001;98(13):7605-7610.
40. Collins, D.P. Cytokine and Cytokine Receptor Expression as a Biological Indicator of Immune Activation: Important Considerations in the Development of In Vitro Model Systems. J Immunol Methods. 2000; 243:125-140.
41. Bartzokis, G., Sultzer D., Mintz, J., Holt, L.E., Marx, P., Phelan, C.K. and Marder S.R. *In vivo* evaluation of brain iron in Alzheimer's disease and normal subjects using MRI. Biol Psychiatry. 1994; 35(7): 480-487.
42. Bartzokis, G., Sultzer D., Cummings, J., Holt, L.E., Hance, D.B., Henderson, V.W. and Mintz, J. *In vivo* evaluation of brain iron in Alzheimer disease using magnetic resonance imaging. Arch Gen Psychiatry. 2000; 57(1): 47-53.
43. Bartzokis, G., Mintz, J., Sultzer D., Marx, P., Herzberg, J.S., Phelan, C.K. and Marder S.R. *In vivo* MR evaluation of age-related increases of brain iron. AJNR Am J Neuroradiol. 1994; 15(6): 1129-1138.
44. Bartzokis, G., Beckson, M., Hance, D.B., Marx, P., Foster, J.A. and Marder S.R. MR evaluation of age-related increase of brain iron in young adult and older normal males. Magn Reson Imaging. 1997; 15(1): 29-35.
45. Chen, J.C., Hardy, P.A., Clauberg, M., Joshi, J.G., Parravano, J., Deck, J.H., Henkelman, R.M., Becker, L.E. and Kucharczyk, W. T2 values in the human brain: comparison with quantitative assays of iron and ferritin. Radiology. 1989; 173(2): 521-526.
46. Gelman, N., Gorell, J.M., Barker, P.B., Savage, R.M., Spickler, E.M., Windham, J.P. and Knight, R.A. MR imaging of human brain at 3.0 T: preliminary report on transverse relaxation rates and relation to estimated iron content. Radiology. 1999; 210(3): 759-767.
47. Jack, C.R. Jr., Petersen, R.C., Xu, Y.C., Waring, S.C., O'Brien, P.C., Tangalos, E.G., Smith, G.E., Ivnik, R.J. and Kokmen, E. Medial temporal atrophy on MRI in normal aging and very mild Alzheimer's disease. Neurology. 1997; 49(3):786-794.
48. Bradbury, M.W.B. Transport of iron in the blood-brain-cerebrospinal fluid system. J Neurochem. 1997;69:443-454.
49. Fenzi, A., Bortolazzi, M., Marzola, P., Colombari, R. *In Vivo* Investigation of Hepatic Iron Overload in Rats Using T2 Maps: Quantification at High Intensity Field (4.7-T). JMRI. *2001*; 13:392-396.
50. Bonkovsky, H.L., Rubin, R.B., Cable, E.E., Davidoff, A., Pels Rijcken, T.H. and Stark, D.D. Hepatic Iron Concentration: Noninvasive Estimation by Means of MR Imaging Techniques. Radiology. 1999; 212:227-234.
51. Ordidge, R.J., Gorell, J.M., Deniau, J.C., Knight, R.A. and Helpern, J.A. Assessment of Relative Brain Iron Concentrations Using T_2-Weighted and T_2*-weighted MRI at 3 Tesla. Magn.Reson.Med. 1994; 32:335-341.
52. Haacke, E.M., Lai, S., Yablonskiy, D.A. and Lin, W. *In Vivo* Validation of the BOLD Mechanism: A Review of Signal Changes in Gradient Echo Functional MRI in the Presence of Flow. Intl J of Imaging Systems and Technology. 1995; 6:153-163.

53. Kiseliev, V.G. and Posse, S. Analytical Model of Susceptibility-induced MR Signal Dephasing: Effect of Diffusion in a Microvascular Network. Magn. Reson. Med. 1999; 41:499-509.
54. Yablonskiy, D.A. and Haacke, E.M. Theory of NMR Signal Behavior in Magnetically Inhomogeneous Tissues: The Static Dephasing Regime. MRM. 1994; 32:749-763.
55. Lin, W., An, H., Celik, A. and Lee, Y. Quantitative Measurements of Cerebral Metabolic Rate of Oxygen ($CMRO_2$) Using MRI. Stroke. 2001 (in press).
56. Petersen, R.C., Stevens, J.C., Ganguli, M. and Tangalos, E.G., Cummings, J.L. and DeKosky S.T. Practice parameter: early detection of dementia: mild cognitive impairment (an evidence-based review). Neurology. 2001; 56:1133-1142.
57. Petersen, R.C. Mild cognitive impairment: transition between aging and Alzheimer's disease. Neurologia. 2000; 15(3): 93-101.
58. Petersen, R.C., Smith, G.E., Waring, S.C., Ivnik, R.J., Tangalos, E.G. and Kokmen, E. Mild cognitive impairment: clinical characterization and outcome. Arch Neurol. 1999; 56(3): 303-308.
59. Johna, S., Kirsch, W. and Robles, A. Laparoscopy-assissted lumboperitoneal shunt: a simplified technique. J Laparascopicendoscopic Surgeons (in press).
60. Fox, N.C. and Rossor, M.N. Diagnosis of early Alzheimer's disease. Rev Neurol. 1999; 155:4S33-4S37.
61. Morris, J.C. The Clinical Dementia Rating (CDR): current version and scoring rules. Neurology. 1993; 43:2412-2414.
62. Van Buskirk. J.J., Kirsch, W.M., Kleyer, D.L., Barkley, R.M. and Koch, T.H. Aminomalonic acid: Identification in *E. coli* and atherosclerotic plaque. . Proc Natl. Acad Sci USA. 1984;81(3):722-725.
63. Green. L.M., Murray, D.K., Tran, D.T., Nelson, G.A., Shah, M.M. and Luben, R.A. A Spontaneously Arising Mutation in Connexin32 with Repeated Passage of FRTL-5 Cells Coincides with Increased Growth Rate and Reduced Thyroxin Release. Mol Endocrinol. 2001, (In press).
64. Yablonskiy, D.A., Reinus, W.R., Stark, H. and Haacke, E.M. Quantitation of T_2' Anisotropic Effects on Magnetic Resonance Bone Mineral Density Measurement. Magnetic Resonance in Medicine. 1996; 36:214-221.
65. Reichenbach, J.R., Venkatesan, R., Schillinger, D.J., Kido, D.K., and Haacke, E.M. Small Vessels in the Human Brain: MR Venography with Deoxyhemoglobin as an Intrinsic Contrast Agent[1]. Radiology. 1997; 204:272-277.
66. Reichenbach, J.R., Venkatesan, R., Yablonskiy, D.A., Thompson, M.R., Lai, S. and Haacke, E. M. Theory and Application of Static Field Inhomogeneity Effects in Gradient-Echo Imaging. JMRI. 1997; 7:266-279.
67. Cheng, N. and Haacke, E.M. Predicting BOLD signal changes as a Function of Blood Volume Fraction and Resolution. NMR in Biomedicine (in press).
68. Haacke, E. M., Lai, S., Reichenbach, J. R., Kuppusamy, K., Hoogenraad, F. G. C., Takeichi, H. and Lin, W. *In Vivo* Measurement of Blood Oxygen Saturation Using Magnetic Resonance Imaging: A Direct Validation of the Blood Oxygen Level-dependent Concept in Functional Brain Imaging. Human Brain Mapping. 1997; 5:341-346.
69. Ogg, R.J., Langston, J.W., Haacke, E.M., Steen, R.G. and Taylor, J.S. The Correlation Between Phase Shifts in Gradient-Echo MR Images and Regional Brain Iron Concentration. Magn.Reson.Imag. 1999; 17:1141-1148
70. LaVaute, T., Smith, S., Cooperman, S., Iwai, K., Land, W., Meyron-Holtz, E., Drake, S.K., Miller, G., Abu-Asab, M., Tsokos, M., Switzer III, R., Grinberg, A., Love, P., Tresser, N., and Rouault, T. Targeted deletion of the gene encoding iron regulatory protein-2 causes missregulation of iron metabolism and neurodegenerative disease in mice. Nature Genetics. .2001; 27:209-214.

71. Kirsch, W.M., Schulz, D. and Leitner, J.W. The effect of prolonged ischemia upon regional energy reserves in the experimental glioblastoma. Cancer Research. 1967; 27(1):2212-2220.
72.. Kirsch, W.M. and Schulz, D.W. Regional bioenergetic events in the experimental glioblastoma. A quantitative histochemical study. J Neurosurg. 1971;34:448-451.
73. Green, L.M., Murray, D.K., Tran, D.T, Bant, A.M., Kazarians, G., Moyers, M.F. and Nelson, G.A. Response of thyroid follicular cells to gamma versus proton irradiation: I. Initial characterization of DNA damage, micronuclei formation, apoptosis, survival and cell cycle phase redistribution. Radiat Res. 2001; 155:32-42.
74. Green, L.M., LaBue, M., Lazarus, J.P. and Colburn, K.K. Characterization of autoimmune thyroiditis in MRL-lpr/lpr mice. Lupus. 1995;4:187-196.
75. Albert, M. The boundary between aging and Alzheimer's disease. Workshop presented at the National Academy of Neuropsychology Annual Meeting, Nov. 15, 2000, Orlando FL.
76. Fox, N.C. and Rossor, M.N. Diagnosis of early Alzheimer's disease. Rev Neurol. 1999; 343(7):33-37.
77. Woohsler, D. WMS-III: Administration and Scoring Manual. The Psychological Corp., San Antonio 1997.
78. Morris, J.C. The Clinical Demential Rating (CDR): Current version and scoring rules. Neurology. 1993;43:2412-2414.
79. Mohs, R.C. and Ferris, S.H. Measuring response to treatment in Alzheimer's disease: what constitutes meaningful change? I J Ger Psychopharm. 1998;1(Suppl 1):S7-S14.
80. Mirra, S.S. The CERAD neurophysiology protocol and consensus recommendations for the postmortem diagnosis of Alzheimer's disease: a commentary. Neurobiol Aging. 1997;18(4 Suppl):S91-S94.
81. Green, L.M., Lazarus, J.P., LaBue, M. and Shah, M.M. Deficient cell-cell communication in a spontaneous murine model of autoimmune thyroiditis. Endocrinol 1995;136(8):3611-3618.
82. Konu, O., Kane, J.K., Barrett, T., Vawter, M.P., Chang, R., Ma, J.Z., Donovan, D.M., Sharp, B., Becker, K.G. and Li, M.D. Region-specific transcriptional response to chronic nicotine in rat brain. Brain Res. 2001;909(1-2):194-203.
83. Manahan, K.J., Taylor, D.D. and Gercel-Taylor, C. Clonal heterogeneity of p53 mutations in ovarian cancer. Int J Oncol. 2001;19(2):387-394.
84. Musso, M., Balestra, P., Bellone, E., Cassandrini, D., Di Maria, E., Lamba Doria, L., Grandis, M., Mancardi, G., Schenone, A., Levi, G., Ajmar, F. and Mandich, P. The D355V mutation decreases EGR2 binding to an element within the Cx32 promoter. Neurobiol Dis. 2001;8(4):700-706.
85. Chen, J.G., Charles, H.C., Barboriak, D.P. and Doraiswamy, P.M. Magnetic resonance spectroscopy in Alzheimer's disease: focus on N-acetylaspartate. Acta Neurol Scan Suppl. 2000;176:20-26.
86. Antuono, P.G., Jones, J.L., Wang, Y. and Li, S.J. Decreased glutamate + glutamine in Alzheimer's disease detected *in vivo* with (1)H-MRS at 0.5 T. Neurology. 2001;56(6):737-742.
87. Valenzuela, M.J. and Sachdev, P. Magnetic resonance spectroscopy in AD. Neurology. 2001;56(5):592-598.
88. Obenaus, A., Yong-Hing, C.J., Tong, K.A., Sarty, G.E. A reliable method for measurement and normalization of pediatric hippocampal volumes. Pediatr Res. 2001;50(1): 124-132.
89. Marsh, L., Morrell, M.J., Shear, P.K., Sullivan, E.V., Freeman, H., Marie, A., Lim, K.O., and Pfefferbaum, A. Cortical and hippocampal volume deficits in temporal lobe epilepsy. Epilepsia. 1997;38:576-587.
90. Lowry, O.H., Passonneau, J.V., Hasselberger, F.X. and Schulz, D.W. Effect of ischemia on known substrates and co-factors of the glycolytic pathway in brain. J Biol Chem. 1964;239:18-30.

91. Lowry, O.H. and Passonneau, J.V. Chapter 11 Dissection and Histological Control. In: A Flexible System of Enzymatic Analysis. 1972, Academic Press, New York, pages 229-235.
92. Jakeman, A., Thompson, T., McHattie, J., Lehotay, C. Sensitive method for nontransferrin-bound iron quantification by graphite furnace atomic absorption spectrometry. Clinical Biochemistry 2001; 34:43-47.